Atmos. Chem. Phys., 14, 1299–1321, 2014
www.atmos-chem-phys.net/14/1299/2014/
doi:10.5194/acp-14-1299-2014

Atmospheric Chemistry and Physics Open Access

Radical chemistry at night: comparisons between observed and modelled HO_x, NO_3 and N_2O_5 during the RONOCO project

D. Stone[1], M. J. Evans[2,3], H. Walker[1], T. Ingham[1,4], S. Vaughan[1], B. Ouyang[5], O. J. Kennedy[5], M. W. McLeod[5], R. L. Jones[5], J. Hopkins[2,3], S. Punjabi[3], R. Lidster[3], J. F. Hamilton[2,3], J. D. Lee[2,3], A. C. Lewis[2,3], L. J. Carpenter[2,3], G. Forster[6], D. E. Oram[6,7], C. E. Reeves[6,7], S. Bauguitte[8], W. Morgan[9,10], H. Coe[9,10], E. Aruffo[11,12], C. Dari-Salisburgo[11], F. Giammaria[12], P. Di Carlo[11,12], and D. E. Heard[1,4]

[1]School of Chemistry, University of Leeds, Leeds, UK
[2]National Centre for Atmospheric Science, University of York, York, UK
[3]Department of Chemistry, University of York, York, UK
[4]National Centre for Atmospheric Science, University of Leeds, Leeds, UK
[5]Department of Chemistry, University of Cambridge, Cambridgeshire, UK
[6]School of Environmental Sciences, University of East Anglia, Norwich, UK
[7]National Centre for Atmospheric Science, University of East Anglia, Norwich, UK
[8]Facility for Airborne Atmospheric Measurements, Bedfordshire, UK
[9]School of Earth Atmospheric and Environmental Science, University of Manchester, Manchester, UK
[10]National Centre for Atmospheric Science, University of Manchester, Manchester, UK
[11]Center of Excellence CETEMPS Universita' degli studi di L'Aquila, L'Aquila, Italy
[12]Dipartimento di Fisica, Universita' degli studi di L'Aquila, L'Aquila, Italy

Correspondence to: D. Stone (d.stone@leeds.ac.uk)

Received: 26 March 2013 – Published in Atmos. Chem. Phys. Discuss.: 11 April 2013
Revised: 9 December 2013 – Accepted: 10 December 2013 – Published: 5 February 2014

Abstract. The RONOCO (ROle of Nighttime chemistry in controlling the Oxidising Capacity of the AtmOsphere) aircraft campaign during July 2010 and January 2011 made observations of OH, HO_2, NO_3, N_2O_5 and a number of supporting measurements at night over the UK, and reflects the first simultaneous airborne measurements of these species. We compare the observed concentrations of these short-lived species with those calculated by a box model constrained by the concentrations of the longer lived species using a detailed chemical scheme. OH concentrations were below the limit of detection, consistent with model predictions. The model systematically underpredicts HO_2 by $\sim$200 % and overpredicts NO_3 and N_2O_5 by around 80 and 50 %, respectively. Cycling between NO_3 and N_2O_5 is fast and thus we define the NO_{3x} ($NO_{3x} = NO_3 + N_2O_5$) family. Production of NO_{3x} is overwhelmingly dominated by the reaction of NO_2 with O_3, whereas its loss is dominated by aerosol uptake of N_2O_5, with NO_3 + VOCs (volatile organic compounds) and $NO_3 + RO_2$ playing smaller roles. The production of HO_x and RO_x radicals is mainly due to the reaction of NO_3 with VOCs. The loss of these radicals occurs through a combination of $HO_2 + RO_2$ reactions, heterogeneous processes and production of HNO_3 from $OH + NO_2$, with radical propagation primarily achieved through reactions of NO_3 with peroxy radicals. Thus NO_3 at night plays a similar role to both OH and NO during the day in that it both initiates RO_x radical production and acts to propagate the tropospheric oxidation chain. Model sensitivity to the N_2O_5 aerosol uptake coefficient ($\gamma_{N_2O_5}$) is discussed and we find that a value of $\gamma_{N_2O_5} = 0.05$ improves model simulations for NO_3 and N_2O_5, but that these improvements are at the expense of model success for HO_2. Improvements to model simulations for HO_2, NO_3 and N_2O_5 can be realised simultaneously on inclusion of additional unsaturated volatile organic compounds, however the nature of these compounds is extremely uncertain.

Published by Copernicus Publications on behalf of the European Geosciences Union.

1 Introduction

Fundamentally the troposphere acts to oxidise emitted compounds through multiple steps until their volatility or solubility drops sufficiently for them to condense to form aerosol, be removed through contact with the ground or by clouds, or be absorbed by the biosphere or oceans. This oxidation chemistry is of fundamental importance for air quality, climate, food security and ecosystem services. Primary pollutants, such as CH_4, volatile organic compounds (VOCs), oxides of nitrogen and SO_2, are removed by oxidation while secondary pollutants such as O_3 and secondary organic aerosol (SOA) are produced as part of the oxidation chain.

During the day, atmospheric oxidation is initiated by photochemical processes, notably the solar photolysis of O_3 to produce electronically excited oxygen atoms ($O(^1D)$) that subsequently react with water vapour to produce OH. Over the last few decades there has been extensive research into the processes producing these oxidants and their subsequent chemistry (see for example Stone et al., 2012 and references therein). Much less emphasis has been placed on understanding nighttime oxidation chemistry and the role of radical species at night.

When primary production of OH by solar photolysis cannot occur, other oxidants dominate, notably O_3 and NO_3 (Mihelcic et al., 1993; Carslaw et al., 1997; Salisbury et al., 2001; Fleming et al., 2006; Warneke et al., 2004; Brown et al., 2009, 2011).

Ozone-initiated oxidation of gas phase compounds is primarily limited to alkenes, where ozonolysis of the C=C double bond initiates the oxidation. Ozonolysis has been investigated in a range of studies in laboratory, chamber and field studies (Salisbury et al., 2001; Fleming et al., 2006; Sommariva et al., 2007; Kanaya et al., 1999, 2002, 2007a; Geyer et al., 2003; Malkin et al., 2010; Johnson and Marston, 2008), and has been shown to be responsible for production of OH and HO_2 radicals at night (Salisbury et al., 2001; Fleming et al., 2006; Sommariva et al., 2007; Kanaya et al., 1999, 2002, 2007a; Emmerson and Carslaw, 2009; Ren et al., 2003, 2006; Volkamer et al., 2010).

The nitrate radical (NO_3) is produced by the reaction between O_3 and NO_2. During the day, NO_3 is rapidly photolysed, leading to low daytime concentrations (Wayne et al., 1991; Brown and Stutz, 2012). However, during the night, NO_3 can accumulate, and a rapid equilibrium with N_2O_5 is established through the production of N_2O_5 via $NO_3 + NO_2$ followed by rapid thermal decomposition of N_2O_5 back to NO_3 and NO_2 (Wayne et al., 1991; Brown and Stutz, 2012). Losses of N_2O_5 are primarily due to reactions on aerosol surfaces, and there is thus much interest in determination of the aerosol uptake coefficient for N_2O_5 on atmospheric aerosols (Brown et al., 2006, 2009, 2011; Escoreia et al., 2010; Tang et al., 2010; Badger et al., 2006; Thornton and Abbatt, 2005; Hallquist et al., 2003; Thornton et al., 2003; Kane et al., 2001; Hu and Abbatt, 1997; Fried et al., 1994; Van Doren et al., 1991; Hanson and Ravishankara, 1991; Mozurkewich and Calvert, 1998). NO_3 radicals can react with a range of species, including alkenes, aldehydes and RO_x radicals (Wayne et al., 1991; Brown and Stutz, 2012).

Although the initiation of nighttime chemistry by the reactions between NO_3 and O_3 with a range of VOCs is relatively well characterised, the subsequent chemistry has received relatively little attention. Measurements of NO_3 have been overestimated by model calculations in several studies (Mihelcic et al., 1993; Sommariva et al., 2006, 2007), with those of nighttime OH and HO_2 radicals typically underestimated, indicating poor understanding of nighttime tropospheric oxidation processes (Kanaya et al., 1999, 2002, 2007a, b; Emmerson and Carslaw, 2009; Geyer et al., 2003; Faloona et al., 2001; Martinez et al., 2003; Ren et al., 2006).

While a number of nighttime studies at ground level close to local sources of NO have observed a limited role of NO_3 in nighttime radical production owing to surface losses of NO_3 and the rapid reaction between NO_3 and NO (Salisbury et al., 2001; Fleming et al., 2006; Sommariva et al., 2007; Kanaya et al., 1999, 2002, 2007a, b; Emmerson and Carslaw, 2009; Faloona et al., 2001; Martinez et al., 2003; Ren et al., 2003, 2005, 2006; Volkamer et al., 2010), several studies of NO_3 and N_2O_5 above ground level and in more remote regions have indicated a more significant role for NO_3 in nighttime radical production and tropospheric oxidation (Platt et al., 1980; Povey et al., 1998; South et al., 1998; Aliwell et al., 1998; Allan et al., 2002; Stutz et al., 2004; Warneke et al., 2004; Brown et al., 2003, 2004, 2006, 2007, 2009, 2011; Aldener et al., 2006; Sommariva et al., 2009; Stutz et al., 2010).

Measurements of NO_3 and N_2O_5 were made downwind of New York City during the New England Air Quality Study (NEAQS) by cavity ringdown spectroscopy (CRDS) onboard the National Oceanic and Atmospheric Administration (NOAA) research vessel (R/V) *Ronald H. Brown* in summers 2002 (Warneke et al., 2004; Brown et al., 2004; Aldener et al., 2006) and 2004 (Sommariva et al., 2009). While measurements of nighttime composition in New York City led to the conclusion that O_3-initiated oxidation processes were dominant at night (Ren et al., 2003, 2006), those made during NEAQS indicated little influence of O_3-initiated VOC oxidation at night, with oxidation of biogenic VOCs dominated by NO_3 (Warneke et al., 2004). Although OH was not measured during NEAQS, the total VOC loss rate owing to reaction with OH over a 24 h period was expected to be $1.7 \times 10^6\,\mathrm{cm^{-3}\,s^{-1}}$, compared to the measured value of $1 \times 10^6\,\mathrm{cm^{-3}\,s^{-1}}$ for NO_3 (Warneke et al., 2004). Conversion of NO_x to HNO_3 at night through NO_3 and N_2O_5 was also found to occur at a comparable rate to that observed during daytime through the $OH + NO_2$ reaction, emphasising the importance of nighttime chemistry for determination of NO_x budgets and O_3 production (Warneke et al., 2004; Brown et al., 2004; Aldener et al., 2006).

Modelling of NEAQS 2004 shipborne data using the Master Chemical Mechanism (MCM) (http://mcm.leeds.ac.uk/MCM/home.htt) (Jenkin et al., 2003; Saunders et al., 2003) demonstrated the importance of peroxy radicals for NO_3 loss, with $NO_3 + RO_2$ reactions representing a median of 15 % of the total calculated NO_3 gas phase loss, and at times up to 60 % of the total NO_3 loss (Sommariva et al., 2006). However, the total sinks for NO_3 and N_2O_5 were still underpredicted, leading to overpredictions of 30–50 % of observed NO_3 and N_2O_5 concentrations (Sommariva et al., 2006).

The NEAQS 2004 aircraft measurements of NO_3 and N_2O_5 were significantly higher than the few ppt typically reported at the surface, with the aircraft observations reaching 400 ppt NO_3 and 3.1 ppb N_2O_5 (Brown et al., 2006, 2007, 2009). The high NO_3 concentrations aloft during NEAQS 2004 resulted in significant nighttime oxidation of isoprene emissions, with $\sim$20 % of isoprene emissions oxidised at night, with over 90 % initiated by NO_3 (Brown et al., 2009). It was suggested that NO_3-initiated oxidation of isoprene could easily dominate isoprene loss on a regional scale, and it was found that isoprene secondary organic aerosol (SOA) mass derived from NO_3 oxidation was 50 % higher than that from OH oxidation (Brown et al., 2009). These observations of NO_3 and N_2O_5 loss processes over a wide range of conditions also demonstrated that the uptake coefficient for N_2O_5 ($\gamma_{N_2O_5}$) on aerosol particles displays a strong dependence on aerosol composition (Brown et al., 2006). A steady state analysis of NO_3 and N_2O_5 sinks (Brown et al., 2003; Brown et al., 2006) indicated that the $\gamma_{N_2O_5}$ can vary by over an order of magnitude, largely dependent on the sulfate mass or sulfate to organic ratio of the aerosol (Brown et al., 2006).

High mixing ratios of NO_3 and N_2O_5 (up to 400 ppt and 2 ppb, respectively) were also reported in a subsequent aircraft study using the NOAA P-3 aircraft during the Texas Air Quality Study (TexAQS) in 2006 (Brown et al., 2011). Budget analyses for the campaign indicated that VOC oxidation at night was rapid, with the total rate of NO_3-initiated oxidation typically 3 to 5 times that initiated by O_3, and NO_3 reactivity indicating the presence of unmeasured plumes of highly reactive VOCs (Brown et al., 2011). Loss of NO_3 was dominated by its chemistry with unsaturated VOCs, with only 14 to 28 % of NO_3 loss occurring indirectly through heterogeneous chemistry of N_2O_5, although significant uncertainties in the N_2O_5 aerosol uptake coefficient were noted (Brown et al., 2011). Reactions of NO_3 with peroxy radicals were estimated as contributing between 1 and 4 % of the total NO_3 loss, although no direct measurements of RO_2 were available, with measurements of PAN (peroxy acetyl nitrate) used to estimate RO_2 concentrations as being equal to the acetylperoxy ($CH_3C(O)O_2$) radical concentration produced by thermal decomposition of PAN (Brown et al., 2011).

Shipborne measurements of NO_3 and total peroxy radicals ($HO_2 + \Sigma RO_2$) were also made during the TexAQS 2006 campaign onboard the R/V *Ronald H. Brown* along the US Gulf Coast (Sommariva et al., 2011). Detailed box modelling of the observations using the MCM showed that $NO_3 + RO_2$ reactions represented, on average, 12–28 % of the total NO_3 sink in relatively unpolluted regions, but that the model underestimated NO_3 and showed high variability in its ability to reproduce observed nighttime concentrations of peroxy radicals (Sommariva et al., 2011).

Previous studies have shown that nighttime chemistry plays a significant role in defining the chemistry of the troposphere. However, there are significant uncertainties in the chemistry of the atmosphere at night. Many of these uncertainties are due to the lack of simultaneous observations of OH, HO_2, NO_3 and N_2O_5. Those observations that do exist often occur within the centres of cities where NO emissions are high, with NO_3 concentrations thus kept low. These "inner city" conditions are not representative of most of the planet and thus do not offer suitable conditions for an evaluation of our understanding of nighttime chemistry.

In this paper we take advantage of simultaneous aircraft measurements of the short-lived species OH, HO_2, NO_3 and N_2O_5, together with the concentrations of long-lived components made away from recent emissions to analyse our understanding of nighttime chemistry as manifested by a constrained box model. Observations of the short-lived species enable assessment of the chemical schemes used in atmospheric models since their concentrations are relatively unaffected by transport processes and are controlled by local chemistry alone (Heard and Pilling, 2003; Stone et al., 2012). Comparison of observed concentrations of short-lived species with calculated concentrations, particularly from detailed box model simulations, thus enables evaluation of our understanding of chemical processes occurring in the atmosphere, making the short-lived species ideal model targets (Heard and Pilling, 2003; Stone et al., 2012).

We provide a brief overview of the campaign in Sect. 2 and measurement techniques in Sect. 3, followed by a description of the model approach in Sect. 4. In Sect. 5 we describe comparisons between modelled and observed concentrations and in Sect. 6 examine the processes controlling atmospheric composition at night. Potential sources of model uncertainty are discussed in Sect. 7, with suggestions for future work in Sect. 8 and conclusions drawn in Sect. 9.

2 The RONOCO Campaign

The ROle of Nighttime chemistry in controlling the Oxidising Capacity of the AtmOsphere (RONOCO) project took place in July 2010 and January 2011. Aircraft measurements were made at altitudes of up to 6400 m over the UK and the North Sea onboard the UK FAAM BAe 146 aircraft, based at East Midlands Airport (52.8° N, 1.3° W) during the campaign. The main objectives of the RONOCO campaign were to obtain comprehensive measurements of nighttime composition to further our understanding of nighttime chemistry thus enabling quantification of the key processes controlling

atmospheric chemistry at night, and ultimately to facilitate assessment of the regional and global impacts of nighttime chemistry on air quality and climate change.

Measurements of HO_x were made on 16 flights throughout the campaign (7 flights in July 2010 and 9 flights in January 2011), while measurements of NO_3 and N_2O_5 were made on 17 flights (9 flights in July 2010 and 8 flights in January 2011). In our analysis we combine all of these flights into a single data set. Figure 1 shows the locations of HO_x, NO_3 and N_2O_5 measurements made during RONOCO. We focus here on the analysis of measurements made at night, defined as periods when the solar zenith angle was greater than 99°, and thus do not include data from flights made in daylight hours or during dawn or dusk periods. Data from flight B537 (20 July 2010) has also been excluded from our analysis owing to a number of atypical observations during this flight which are discussed elsewhere (Kennedy et al., 2011; Walker et al., 2014).

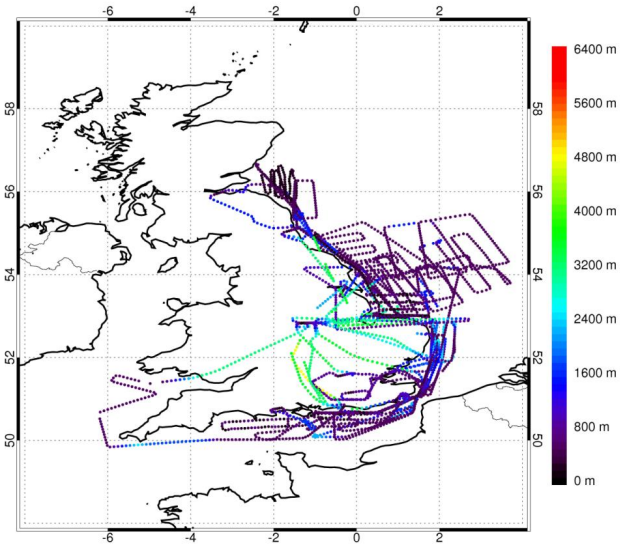

Fig. 1. Locations of the BAe 146 aircraft during the RONOCO campaign for which measurements of HO_2* and NO_3 or N_2O_5 are available, coloured by altitude.

3 Measurements during RONOCO

3.1 Detection of OH and HO_2

OH and HO_2 radicals were measured by laser-induced fluorescence (LIF) spectroscopy at low pressure using the fluorescence assay by gas expansion (FAGE) technique (Heard and Pilling, 2003). The instrument has been described in detail elsewhere (Commane et al., 2010; Stone et al., 2011), and only a brief description is given here.

Ambient air from the aircraft exterior is drawn into a fluorescence cell maintained at pressures ranging from 1.9 Torr at sea level to 1.2 Torr at 6 km altitude. The fluorescence cell has two excitation axes, with excess NO added at the second axis to titrate HO_2 to OH, enabling simultaneous detection of OH and HO_2. OH radicals in both excitation axes are excited by laser light at $\lambda \sim 308$ nm, generated by a solid state Nd:YAG (neodymium yttrium aluminum garnet) pumped Ti:sapphire laser system which is frequency tripled (Bloss et al., 2003). Channel photomultiplier tubes coupled to gated photon counters were used to detect the $A^2\Sigma^+ - X^2\Pi_i$ OH fluorescence signal at $\lambda \sim 308$ nm.

Calibration of the instrument is achieved by measurement of the fluorescence signal from known concentrations of OH and HO_2, produced by the photolysis of water vapour, and was performed over a range of conditions before and after the RONOCO campaign. The instrument sensitivity to OH (C_{OH}) was determined to be $(2.9 \pm 0.45) \times 10^{-8}$ s^{-1} cm^3 mW^{-1} for the summer campaign and $(4.3 \pm 0.7) \times 10^{-8}$ s^{-1} cm^3 mW^{-1} for the winter campaign. The instrument sensitivity to HO_2 (C_{HO_2}) was determined to be $(0.9 \pm 1.5) \times 10^{-7}$ s^{-1} cm^3 mW^{-1} for the summer campaign and $(1.2 \pm 0.21) \times 10^{-7}$ s^{-1} cm^3 mW^{-1} for the winter campaign. Calibration uncertainties (1σ) are on the order of 15 to 20 % for OH and HO_2. For OH, the 1σ limit of detection (LOD) was 1.8×10^6 cm^{-3} for a 5 min averaging period during the summer campaign and 6.4×10^5 cm^{-3} during the winter campaign. The HO_2 1σ LOD was 6.9×10^5 cm^{-3} for a 4 min averaging period during the summer and 6.0×10^5 cm^{-3} during the winter, and is better than that for OH owing to lower losses on the walls of the sampling tube following the supersonic expansion. While instrument sensitivity does vary with the pressure in the detection cells, and thus with altitude, the cell pressures during RONOCO varied by less than 0.7 Torr (in the range 1.2–1.9 Torr). As discussed in detail by Commane et al. (2010), pressure dependent calibrations of the instrument are achieved by varying cell pressure using different sized pinholes through which ambient air is drawn into the instrument to control the flow of gas in the cell. Over the range of cell pressures encountered during RONOCO, there is little variation of C_{OH} or C_{HO_2} (Commane et al., 2010), and values reported here are thus the mean values determined during calibrations in this pressure range. Uncertainties associated with measurements of OH and HO_2 are 28–35 % (1σ) and include the calibration uncertainites. Further details regarding the FAGE instrument and calibration procedures will be provided by Walker et al. (2014).

3.2 Detection of NO_3 and N_2O_5

NO_3 and N_2O_5 were detected by broadband cavity enhanced absorption spectroscopy (BBCEAS), as described in detail by Kennedy et al. (2011). Briefly, air is drawn into three 94 cm-long high finesse optical cavities, with each bound by two highly reflective mirrors, which are irradiated with collimated light from an incoherent broadband continuous wave

light source. Each cavity is coupled to a spectrometer interfaced to a charge coupled device (CCD) detector by fibre optic bundles, where the wavelength dependent light intensity transmitted through the cavity is recorded.

NO_3 is identified and measured via its strong $B^2E'-X^2A'_2$ electronic transition centred around 662 nm, with light provided by a red light emitting diode (LED). N_2O_5 is measured in a separate cavity maintained at 80 °C following its thermal dissociation to NO_3 and NO_2 at 120 °C in a heater situated prior to the cavity entrance, and thus measured as the sum of ambient NO_3 and thermally dissociated N_2O_5. The third cavity enables detection of NO_2 using light provided by a blue LED with output centred around 460 nm.

A crystalline source of N_2O_5, stabilised at temperatures between −80 and −77 °C, was used to provide known amounts of NO_3 and N_2O_5 to facilitate calibration of the instrument in the laboratory. The in-flight 1σ LOD (determined at a pressure of 0.7 bar) for NO_3 was found to be 1.1 ppt for a 1 s integration time, with a corresponding LOD of 2.4 ppt for the sum of $NO_3 + N_2O_5$.

3.3 Supporting measurements

Measurements from several other instruments onboard the BAe 146 during the RONOCO campaign have been used in the analysis presented here. Details of these supporting measurements are summarised in Table 1.

4 Model approach

Observations of OH, HO_2, NO_3 and N_2O_5 have been interpreted using the Dynamically Simple Model of Atmospheric Chemical Complexity (DSMACC), which is described in detail by Emmerson and Evans (2009) and Stone et al. (2010). DSMACC is a zero-dimensional model using the kinetic pre-processor (KPP) (Sandu and Sander, 2006), and in this work uses a chemistry scheme described by the MCM v3.2 (http://mcm.leeds.ac.uk/MCM/home.htt) (Jenkin et al., 2003; Saunders et al., 2003). The full MCM contains near explicit degradation schemes for 143 primary species, resulting in 6700 species in approximately 17 000 reactions and representing the most detailed and comprehensive chemistry scheme available for modelling tropospheric composition. Simulations reported here use degradation chemistry for ethane, propane, *iso*-butane, *n*-butane, *iso*-pentane, *n*-pentane, sum of 2+3-methylpentane, *n*-hexane, *n*-heptane, *n*-octane, ethene, propene, acetylene, *trans*-2-butene, 1-butene, *cis*-2-butene, *iso*-butene, 1,3-butadiene, *trans*-2-pentene, 1-pentene, isoprene, benzene, toluene, ethylbenzene, xylene, methacrolein and acetone. The scheme used contains ∼ 2000 species in ∼ 8000 reactions.

Heterogeneous loss of several species (OH, HO_2, CH_3O_2, NO_3, N_2O_5 and HNO_3) to aerosol surfaces was represented in the model by parameterisation of a first-order loss process to the aerosol surface (Schwarz, 1986):

$$k' = \left(\frac{r}{D_g} + \frac{4}{\gamma_x c_g}\right)^{-1} A, \quad (1)$$

where k' is the first-order rate coefficient for heterogeneous loss, r is the aerosol particle effective radius, D_g is the gas phase diffusion coefficient (Eq. 2), γ_x is the uptake coefficient for species X, c_g is the mean molecular speed (Eq. 3), and A is the aerosol surface area per unit volume. D_g is given by

$$D_g = \frac{3}{N_A d_g^2 \rho_{air}} \sqrt{\frac{RT m_{air}}{2\pi} \left(\frac{m_g + m_{air}}{m_g}\right)}, \quad (2)$$

where N_A is Avogadro's number, d_g is the diameter of the gas molecule, ρ_{air} is the density of air, R is the gas constant, and m_g and m_{air} are the molar masses of gas and air, respectively. c_g is given by

$$c_g = \left(\frac{8RT}{\pi M_w}\right)^{1/2}, \quad (3)$$

where T is the temperature and M_w is the molecular weight of the gas. For HO_2, $\gamma_{HO_2} = 0.028$ is used based on the mean value reported by the parameterisation by Macintyre and Evans (2011). For NO_3, a value of $\gamma_{NO_3} = 0.001$ is used. For N_2O_5, $\gamma_{N_2O_5} = 0.02$ is used in our base simulations, based on the mean value reported from the parameterisation by Evans and Jacob (2005). Model sensitivity to $\gamma_{N_2O_5}$ is discussed in Sect. 7.2.

An additional first-order loss process for each species in the model is also included to represent deposition processes, with the first-order rate set to be equivalent to a lifetime of approximately 24 h. Model sensitivity to this parameter is discussed in Sect. 7.1.

All aircraft measurements are merged onto a 60 s timebase. Time points with observations of OH or HO_2 are modelled if observations of physical state (latitude, longitude, pressure, temperature and water vapour concentration), aerosol surface area and concentrations of CO, O_3, NO_2, NO_3 and VOCs are available. We perform 1648 simulations in total. For each 60 s time period, we use the observed concentrations of the constrained species, appropriately averaged over that time period, to run the simulation. We then compare with the appropriately averaged values of HO_2, NO_3 and N_2O_5 over that time period. A summary of species used to constrain the model is given in Table 2. Observed concentrations of CO, O_3, H_2O, VOCs and aerosol surface area for each 60 s time point are fixed and held constant throughout the corresponding model run, with concentrations of CH_4 and H_2 kept constant at values of 1770 (NOAA CMDL flask analysis, ftp://ftp.cmdl.noaa.gov/ccg/ch4/) and

Table 1. Supporting measurements made onboard the BAe 146 aircraft during the RONOCO project and used in the model analysis presented here. [a] The NO_2 measurements used to constrain the model were made by the LIF instrument (Dari-Salisburgo et al., 2009; Di Carlo et al., 2013). ΣANs – sum of alkyl nitrates; ΣPNs – sum of peroxy nitrates; PAN – peroxy acetyl nitrate; VOCs – volatile organic compounds. [b] Aerosol surface area is estimated for ambient relative humidity based on the measured dry size distribution and composition. [c] The total surface area SMPS + PCASP is within 10 % of the total using the SMPS data alone. Note that the aerosol measurements do not show any evidence for enhanced coarse model aerosol at low altitudes, indicating the aircraft did not enter the marine boundary layer.

Species measured	Technique	Time resolution and limit of detection (LOD)	Reference
OH, HO_2	Detection of OH by LIF using FAGE; conversion of HO_2 to OH in excess NO, detection of OH by LIF-FAGE.	For OH, 1.8×10^6 cm^{-3} LOD for a 5 min averaging period during summer; 6.4×10^5 cm^{-3} during winter. For HO_2, 6.9×10^5 cm^{-3} LOD for a 4 min averaging period during summer; 6.0×10^5 cm^{-3} during winter.	Commane et al. (2010)
NO_3, N_2O_5	BBCEAS of NO_3; thermal dissociation of N_2O_5 to $NO_3 + NO_2$, detection of NO_3 by BBCEAS.	1 s resolution; 1.1 ppt LOD for NO_3; 2.4 ppt LOD for NO_3+N_2O_5.	Kennedy et al. (2011)
CO	Aero Laser AL5002 Fast Carbon Monoxide Monitor.	3.5 ppb LOD at 1 s resolution.	Gerbig et al. (1999)
O_3	TECO 49C UV absorption.	1 s resolution; 0.6 ppb LOD.	Hewitt et al. (2010)
NO, NO_2[a]	FAAM fast NO_x instrument; TECO 42C analyser using heated molybdenum filament to convert NO_2 to NO with detection of NO by chemiluminescence.	10 s resolution; 3 ppt LOD for NO, 15 ppt LOD for NO_2.	Brough et al. (2003)
NO_2[a], ΣANs, ΣPNs	Thermal decomposition of ΣANs and ΣPNs to NO_2; detection of NO_2 by LIF.	1 s resolution; LODs 9.8 ppt for NO_2, 28.1 ppt for ΣANs, 18.4 ppt for ΣPNs.	Dari-Salisburgo et al. (2009); Di Carlo et al. (2013)
PAN	Gas chromatography with electron capture detection.	90 s resolution; 5 ppt LOD.	Whalley et al. (2004)
VOCs	Gas chromatography with flame ionisation detection (GC-FID).	Variable.	Hopkins et al. (2003)
Aerosol surface area[b]	SMPS for particles of diameter 20–350 nm and passive cavity aerosol spectrometer probe (PCASP) for particles with diameter > 350 nm[c].	60 s resolution; uncertainty of ±30 %.	Hewitt et al. (2010); Wiedensohler et al. (2012)

550 ppb (Ehhalt and Rohrer, 2009; Novelli et al., 1999) respectively. Species which were not observed are set initially to zero in the model.

Constraints on nitrogen oxides (NO, NO_2, NO_3, N_2O_5, HONO and HO_2NO_2) were applied using the method described by Stone et al. (2010), with the primary constraint placed on NO_2. Thus, the initial concentration of NO_2 in the model is set to its observed value and the concentrations of all nitrogen oxide species, including NO_2, are permitted to vary according to their photochemistry as the model runs forwards. At the end of each 24 h period in the model, the calculated concentration of NO_2 is compared to its observed concentration, and the concentrations of all nitrogen oxide species are fractionally increased or decreased such that the modelled and observed concentrations of NO_2 are the same. The model is integrated forwards in time with diurnally varying photolysis rates until a diurnal steady state is reached, typically requiring between 5 and 10 days. Thus at the point of comparison between the model and observations we have a modelled NO_2 concentration equal to the observed concentration, together with concentrations of the other NO_x species (NO, NO_3, N_2O_5, HONO, HO_2NO_2) consistent with that NO_2 concentration, the concentration of the other measured species, and the time since darkness fell.

Following the work of Fuchs et al. (2011), model calculations described in this work include representation of potential RO_2 interferences in LIF measurements of HO_2. We thus describe observed to modelled comparisons of

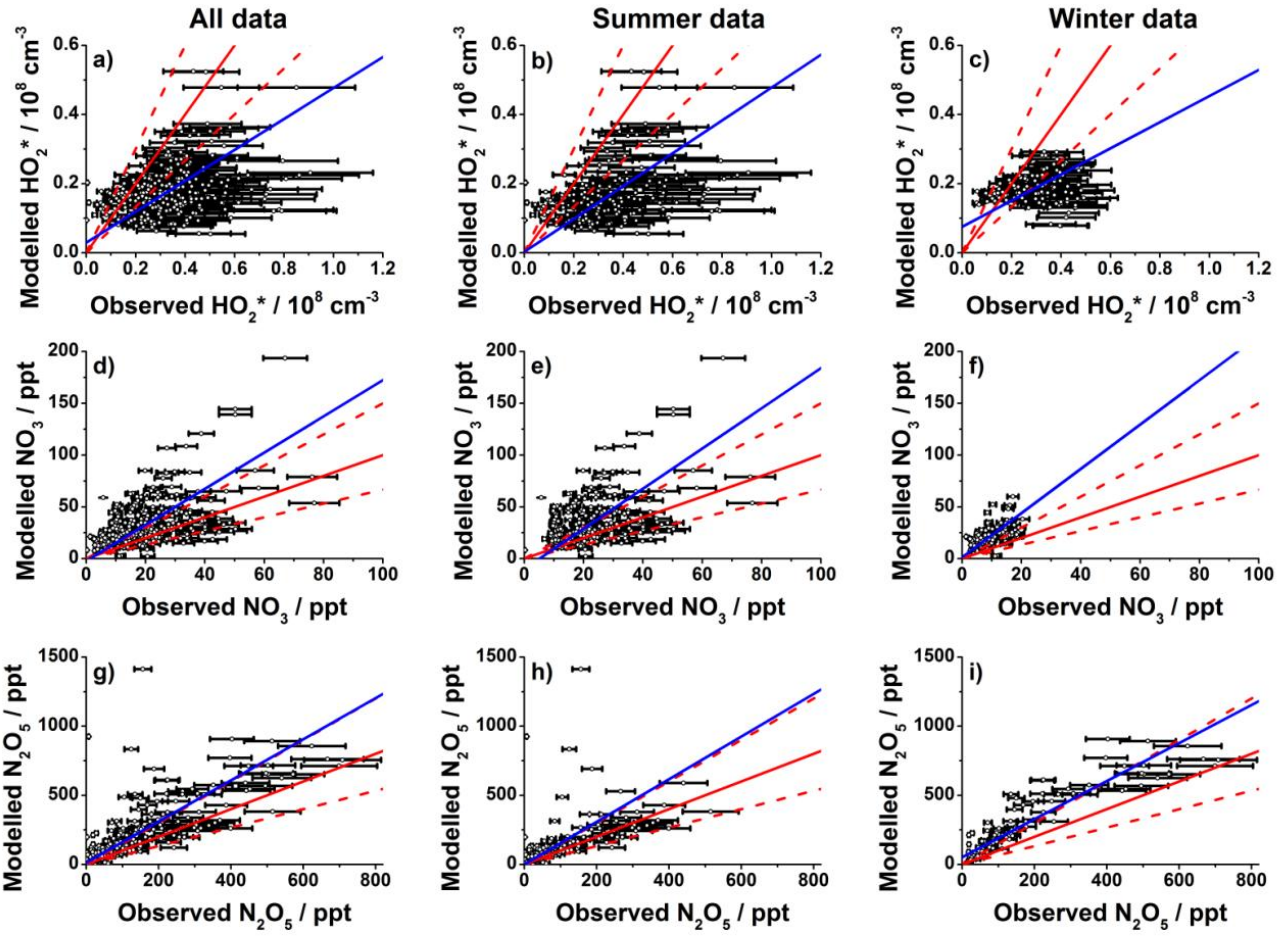

Fig. 2. Comparison of modelled and observed concentrations of **(a)** HO_2* (all data), $[HO_2^*]_{mod} = \{(0.5 \pm 0.1) \times [HO_2^*]_{obs}\} + (3.0 \pm 2.2) \times 10^6\,cm^{-3}$ ($r^2 = 0.1$); **(b)** HO_2* (summer data), $[HO_2^*]_{mod} = \{(0.5 \pm 0.1) \times [HO_2^*]_{obs}\} + (0.3 \pm 3.1) \times 10^6\ cm^{-3}$ ($r^2 = 0.1$); **(c)** HO_2* (winter data), $[HO_2^*]_{mod} = \{(0.4 \pm 0.2) \times [HO_2^*]_{obs}\} + (7.5 \pm 4.4) \times 10^6\ cm^{-3}$ ($r^2 = 0.02$); **(d)** NO_3 (all data), $[NO_3]_{mod} = \{(1.8 \pm 0.2) \times [NO_3]_{obs}\} - (2.3 \pm 3.6)$ ppt ($r^2 = 0.3$); **(e)** NO_3 (summer data), $[NO_3]_{mod} = \{(2.0 \pm 0.3) \times [NO_3]_{obs}\} - (9.9 \pm 6.0)$ ppt ($r^2 = 0.2$); **(f)** NO_3 (winter data), $[NO_3]_{mod} = \{(2.2 \pm 0.4) \times [NO_3]_{obs}\} + (1.3 \pm 4.1)$ ppt ($r^2 = 0.3$); **(g)** N_2O_5 (all data), $[N_2O_5]_{mod} = \{(1.5 \pm 0.1) \times [N_2O_5]_{mod}\} - (42.4 \pm 19.7)$ ppt ($r^2 = 0.6$); **(h)** N_2O_5 (summer data), $[N_2O_5]_{mod} = \{(1.6 \pm 0.2) \times [N_2O_5]_{mod}\} - (0.2 \pm 18.1)$ ppt ($r^2 = 0.3$); **(i)** N_2O_5 (winter data), $[N_2O_5]_{mod} = \{(1.4 \pm 0.2) \times [N_2O_5]_{mod}\} + (52.4 \pm 43.2)$ ppt ($r^2 = 0.8$). In each plot, the solid red line indicates the 1 : 1 line, with 50 % limits given by the broken red lines. The best fit lines are shown in blue. Errors bars are 1σ.

HO_2*, where $HO_2^* = HO_2 + fRO_2$, with the factor f derived from a combination of experimental parameters and MCM chemistry, as described in the appendix. For the RONOCO campaign, potential interferences in HO_2 measurements are expected to be small on average, with $HO_2^* = [1.15 \times HO_2] + 2 \times 10^5\,cm^{-3}$.

5 Model performance

Figures 2 and 3 show the model performance for HO_2*, NO_3 and N_2O_5. Modelled concentrations of OH were on the order of $10^4\,cm^{-3}$ (mean $= (2.4 \pm 2.3) \times 10^4\,cm^{-3}$; median $= 1.7 \times 10^4\,cm^{-3}$) and were consistently below the 1σ instrumental limits of detection of $1.8 \times 10^6\,cm^{-3}$ in summer and $6.4 \times 10^5\,cm^{-3}$ in winter (for 5 min averaging periods). We do not consider the model performance for OH in any more detail.

The model displays a tendency to underpredict HO_2* and overpredict NO_3 and N_2O_5, as shown in Fig. 2. For HO_2*, the line of best fit for the campaign average is given by $[HO_2^*]_{mod} = \{(0.5 \pm 0.1) \times [HO_2^*]_{obs}\} + (3.0 \pm 2.2) \times 10^6\,cm^{-3}$ ($r^2 = 0.1$), with the campaign average for NO_3 given by $[NO_3]_{mod} = \{(1.8 \pm 0.2) \times [NO_3]_{obs}\} - (2.3 \pm 3.6)$ ppt ($r^2 = 0.3$) and the campaign average best fit line for N_2O_5 described by $[N_2O_5]_{mod} = \{(1.5 \pm 0.1) \times [N_2O_5]_{mod}\} - (42.4 \pm 19.7)$ ppt ($r^2 = 0.6$). As shown in Fig. 2, similar model behaviour is observed for the winter and

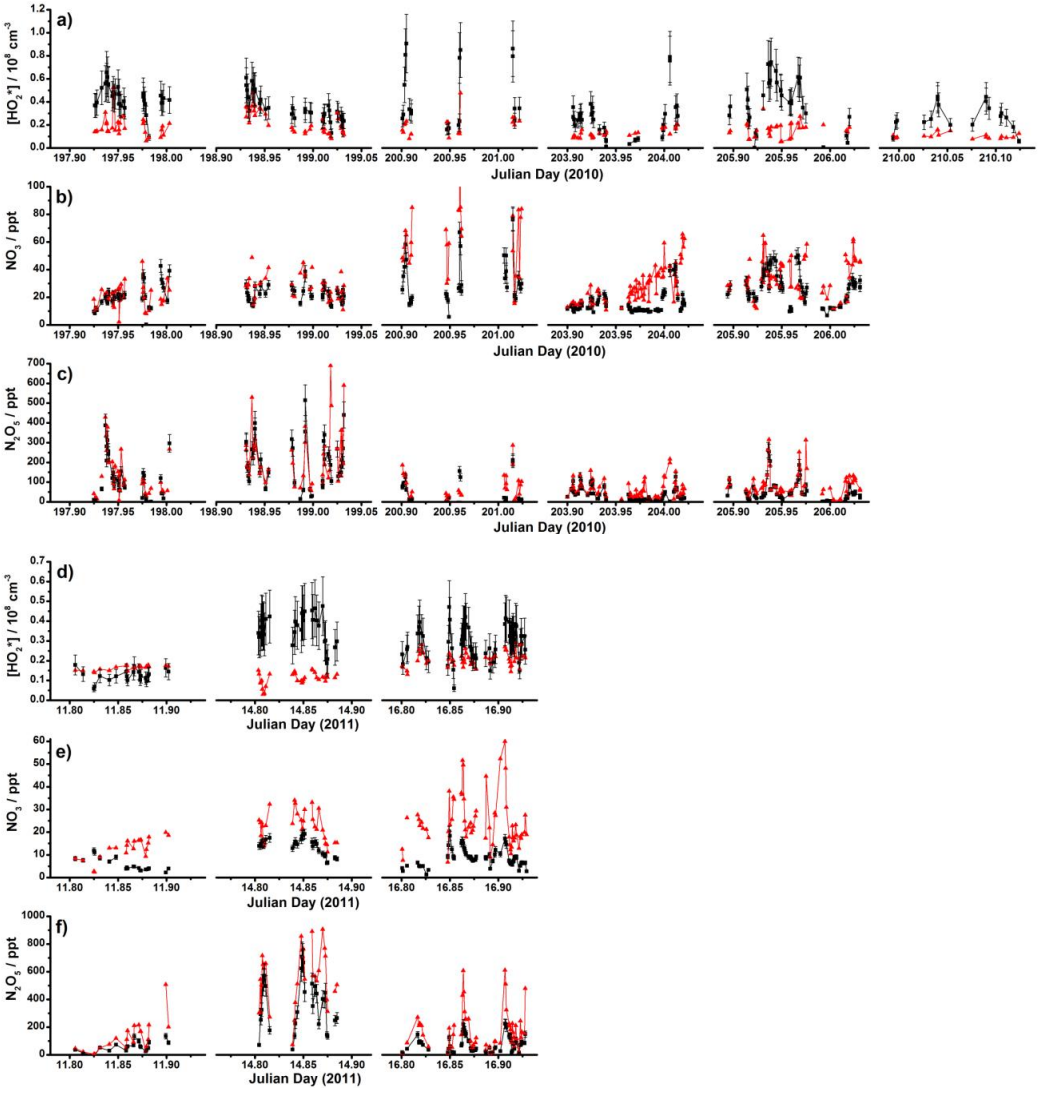

Fig. 3. Time series of observed (black) and modelled (red) concentrations of **(a)** HO_2* during the summer campaign, **(b)** NO_3 during the summer campaign, **(c)** N_2O_5 during the summer campaign, **(d)** HO_2* during the winter campaign, **(e)** NO_3 during the winter campaign, and **(f)** N_2O_5 during the winter campaign. Errors bars are 1σ. Data for NO_3 and N_2O_5 above 100 and 1000 ppt, respectively, are not shown for clarity (< 6 data points in total).

summer campaigns. The modelled lifetime of HO_2* was $(209 \pm 52)\,s^{-1}$ on average for the entire data set (median = $209\,s^{-1}$), $(198 \pm 52)\,s^{-1}$ (median = $200\,s^{-1}$) for the summer campaign, and $(223 \pm 49)\,s^{-1}$ (median = $216\,s^{-1}$) for the winter campaign. For NO_3, the modelled lifetime was $(51 \pm 59)\,s^{-1}$ on average for the entire data set (median = $35\,s^{-1}$), $(46 \pm 40)\,s^{-1}$ (median = $36\,s^{-1}$) for the summer campaign, and $(60 \pm 88)\,s^{-1}$ (median = $30\,s^{-1}$) for the winter campaign. For N_2O_5, the modelled lifetime was $(147 \pm 124)\,s^{-1}$ on average for the entire data set (median = $101\,s^{-1}$), $(88 \pm 29)\,s^{-1}$ (median = $85\,s^{-1}$) for the summer campaign, and $(284 \pm 148)\,s^{-1}$ (median = $221\,s^{-1}$) for the winter campaign.

Figure 4 shows the modelled to observed ratios for HO_2*, NO_3 and N_2O_5 as a function of altitude. Since the majority of data were recorded over a small altitude range, there is little evidence of any relationship between model success and altitude. The relationships between the modelled to observed ratios for N_2O_5 and NO_3, HO_2 and NO_3, and HO_2 and N_2O_5, are given in Fig. 5.

Model underpredictions for nighttime HO_2 of a similar magnitude have been observed in a number of previous studies, and, where observations are available, model underpredictions of HO_2 tend to coincide with underpredictions of RO_2 and overpredictions of NO_3. Measurements of peroxy radicals in the Black Forest, Germany, were underestimated by a factor of 3–4, coinciding with an overprediction of NO_3

Table 2. Summary of observations used to constrain the model in this work and, in the case of HO_2*, NO_3 and N_2O_5, to compare with model calculations. Zero values indicate measurements below the instrumental limits of detection.

Species	Mean $\pm 1\sigma$	Median	Range
O_3/ppb	37.0 ± 8.1	35.5	11–63
CO/ppb	110.4 ± 27.1	99.9	71–250
H_2O/ppm	$10\,418 \pm 2425$	10 491	178–15 509
NO_2/ ppt	1614.4 ± 1749.2	946.7	66–14 570
NO/ppt	24.6 ± 278.9	0	0–4501
ethane/ppt	1109.5 ± 882.0	940.8	0–3208
propane/ppt	414.0 ± 416.5	235.9	0–1770
iso-butane/ppt	94.4 ± 91.3	73.0	0–372
n-butane/ppt	171.7 ± 162.2	140.8	0–726
iso-pentane/ppt	80.9 ± 139.6	70.5	0–2176
n-pentane/ppt	50.4 ± 57.1	38.4	0–455
methylpentanes/ppt	28.3 ± 31.2	21.3	0–224
n-hexane/ppt	17.0 ± 18.3	11.9	0–135
n-heptane/ppt	6.9 ± 10.1	5.7	0–146
n-octane/ppt	2.6 ± 4.5	0	0–45
ethene/ppt	130.5 ± 121.2	117.6	0–590
propene/ppt	30.9 ± 45.4	12.0	0–239
acetylene/ppt	158.9 ± 161.0	96.8	0–516
trans-2-butene/ppt	3.2 ± 2.1	3.8	0–10
1-butene/ppt	6.7 ± 7.7	5.5	0–75
iso-butene/ppt	5.4 ± 8.4	4.9	0–137
cis-2-butene/ppt	0.1 ± 0.6	0	0–7
1,3-butadiene/ppt	2.8 ± 17.1	0	0–230
trans-2-pentene/ppt	0.1 ± 0.7	0	0–11
1-pentene/ppt	0.9 ± 2.5	0	0–24
isoprene/ppt	0.9 ± 3.2	0	0–40
benzene/ppt	47.9 ± 58.7	21.1	0–458
toluene/ppt	40.5 ± 57.1	34.0	0–773
ethylbenzene/ppt	8.5 ± 13.3	6.0	0–178
m-xylene/ppt	18.1 ± 42.1	6.4	0–693
o-xylene/ppt	6.1 ± 17.2	0	0–268
methacrolein/ppt	7.3 ± 27.9	0	0–325
acetone/ppt	444.0 ± 616.0	257.9	0–8073
PAN/ppt	31.2 ± 44.2	19.0	0–234
HO_2*/10^8 cm^{-3}	0.33 ± 0.16	0.32	0.001–0.91
NO_3/ppt	18.9 ± 12.0	16.16	0.29–76.85
N_2O_5/ppt	119.87 ± 131.02	72.0	6.35–726.353

by a factor of ~ 2, with discrepancies for both NO_3 and peroxy radicals reconciled by consideration of the impact of unmeasured monoterpenes (Mihelcic et al., 1993). Observations of HO_2 at night on Rishiri Island, Japan, were strongly correlated with monoterpene emissions (Kanaya et al., 2002, 2007a) and were also generally underestimated by model calculations (Kanaya et al., 1999, 2002, 2007). Model calculations for the Southern Oxidant Study (SOS) in Nashville, USA, underpredicted nighttime observations of HO_2 by factors of 2–8, partly owing to the limited $NO_3 + VOC$ and $NO_3 + RO_2$ chemistry in the model (Martinez et al., 2003). Model underpredictions for nighttime HO_2 have also been reported for campaigns near London (Emmerson and Carslaw, 2009), in New York (Ren et al., 2003, 2006) and Tokyo (Kanaya et al., 2007b), with investigation of the model discrepancy for the Tokyo campaign indicating the presence of unmeasured VOCs which, if included in the model, could reconcile the modelled HO_2 with the observations (Kanaya et al., 2007). The presence of unmeasured VOCs was also thought to be responsible for discrepancies between observed concentrations of NO_3 and calculations of NO_3 reactivity from measured sources and sinks during the TexAQS campaign (Brown et al., 2011).

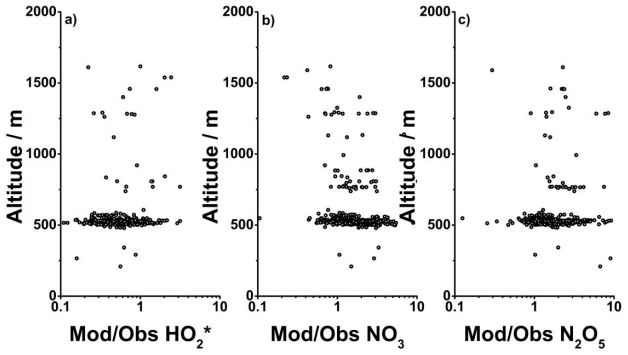

Fig. 4. Modelled to observed ratios as a function of altitude for **(a)** HO_2*, **(b)** NO_3 and **(c)** N_2O_5. There are limited data above altitudes of 2000 m, and data above 2000 m are not shown for clarity.

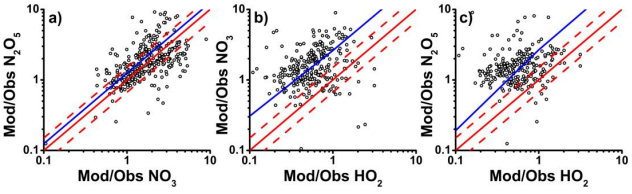

Fig. 5. Relationships between modelled to observed ratios for **(a)** NO_3 and N_2O_5, **(b)** HO_2* and NO_3, and **(c)** HO_2* and N_2O_5 for summer and winter data combined. In each plot, the solid red line indicates the 1 : 1 line, with 50 % limits given by the broken red lines. The best fit lines are given in blue, and are described by **(a)** $y = (1.3 \pm 0.2)x - (0.4 \pm 0.3)$, $r^2 = 0.2$; **(b)** $y = (2.6 \pm 0.5)x + (0.3 \pm 0.1)$, $r^2 = 0.1$; and **(c)** $y = (2.8 \pm 0.7)x - (0.1 \pm 0.5)$, $r^2 = 0.02$.

In order to show the important processes occurring within the model and to thus provide insights into improving model fidelity we now diagnose the chemical processes occurring within the model. We start our analysis with the budgets of NO_3 and N_2O_5, we then turn our attention to the wider RO_x family and finally to HO_x, HO_2 and OH.

6 Budget analyses

6.1 NO_3 and N_2O_5 budgets

NO_3 and N_2O_5 rapidly interconvert through the reaction of NO_3 with NO_2 and thermal decomposition of N_2O_5, with the interconversion occurring at a faster rate (3.4×10^7 cm^{-3} s^{-1}

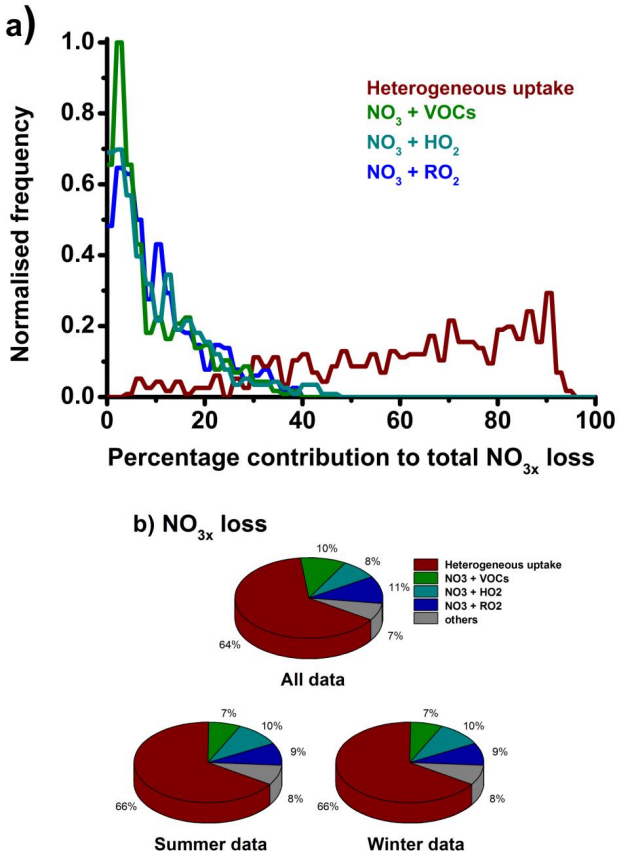

Fig. 6. Processes controlling losses of NO_{3x} (i.e. $NO_3 + N_2O_5$) in the model, displayed as **(a)** the probability distribution functions for the percentage contributions to the total loss for heterogeneous uptake of NO_{3x} to aerosol surfaces (red), $NO_3 + VOCs$ (green), $NO_3 + HO_2$ (light blue) and $NO_3 + RO_2$ (all organic peroxy radicals) (dark blue); and **(b)** the summer and winter campaign means combined (upper panel), summer campaign mean (lower panel, left hand side) and winter campaign mean (lower panel, right hand side). The average total loss rate of NO_{3x} was $(7.8 \pm 6.9) \times 10^5$ cm^{-3} s^{-1} (median $= 5.5 \times 10^5$ cm^{-3} s^{-1}) for the entire data set, $(7.6 \pm 6.6) \times 10^5$ cm^{-3} s^{-1} (median $= 5.5 \times 10^5$ cm^{-3} s^{-1}) for the summer campaign and $(8.2 \pm 7.7) \times 10^5$ cm^{-3} s^{-1} (median $= 6.0 \times 10^5$ cm^{-3} s^{-1}) for the winter campaign.

on average during RONOCO, with a range of 1.0×10^5 to 9.3×10^8 cm^{-3} s^{-1} and median of 2.2×10^7 cm^{-3} s^{-1}) than the conversion between OH and HO_2 (4.5×10^4 cm^{-3} s^{-1} on average during RONOCO, with a range of 2.9×10^3 to 4.6×10^5 cm^{-3} s^{-1} and median of 4.0×10^4 cm^{-3} s^{-1}). This leads us to define the NO_{3x} family, where $NO_{3x} = NO_3 + N_2O_5$. Production of NO_{3x} occurs almost exclusively through the production of NO_3 by $O_3 + NO_2$, with minor production channels (< 0.01 %) including $OH + HNO_3$ and reactions of Criegee biradicals with NO_2.

Figure 6 shows the loss pathways for NO_{3x} at night, displayed as the probability distribution functions for the percentage contribution of each process to the total NO_{3x} loss. The largest loss of NO_{3x} is typically due to heterogeneous processes, through the uptake and hydrolysis of N_2O_5 on aerosol surfaces, representing 64 % of the total NO_{3x} loss averaged over all simulated data points. However, there is high variability in the fraction of the total loss through heterogeneous processes, as displayed in Fig. 6. Reactions of NO_3 with VOCs comprise 10 % of the total NO_{3x} loss on average, with a maximum value of 40 % when VOC concentrations are high and aerosol loadings low. Loss of NO_{3x} through reactions of NO_3 with peroxy radicals represents 19 % of the total (11 % from organic RO_2 and 8 % from HO_2) on average, but there are data points where the loss of NO_{3x} through such reactions reaches 71 %, with separate budget analyses for the winter and summer campaigns resulting in similar conclusions to the campaign average. Thus, although in a mean sense the loss of NO_{3x} from the atmosphere is dominated by the heterogeneous uptake of N_2O_5 onto aerosol, there are significant other processes which can dominate under certain conditions.

These results are consistent with previous studies. Modelling of the NEAQS 2004 shipborne campaign using the MCM revealed similar losses of NO_3 to RO_2 in the marine boundary layer to those presented here, with a mean contribution of 19 % to the total gas phase NO_3 loss and a maximum of up to 60 % (Sommariva et al., 2009). In contrast, analysis of NO_3 budgets for the airborne TexAQS 2006 campaign suggested that only 1–4 % of the total NO_{3x} loss occurred as a result of reactions of NO_3 with peroxy radicals (Brown et al., 2011). However, no peroxy radical measurements were made during TexAQS, and RO_2 concentrations were estimated using observations of PAN and its thermal decomposition rate, and were thus almost certainly a significant underestimate, as noted in the analysis (Brown et al., 2011). Model calculations in this work indicate that the peroxy radical derived from thermal decomposition of PAN represents a maximum of 15 % of the total organic peroxy radical concentration during RONOCO, with a median value of 0.3 %.

6.2 RO_x radical budgets

RO_x ($RO_2 + RO + HO_2 + OH$) radicals play a central role in the nighttime chemistry of the troposphere. Figure 7 shows the production and loss processes for RO_x radicals at night during RONOCO (note that the discussion in this section concerns HO_2 and not HO_2*). Initiation of radicals at night, and thus of nighttime oxidation chemistry, is dominated by reactions of NO_3 with unsaturated VOCs, with a mean campaign contribution of 80 % compared to 18 % for radical production by alkene ozonolysis reactions. Figure 8 shows that of the VOCs measured during the campaign (Table 2), the dominant species in terms of NO_3 reactivity are *iso*-butene (36 %), *trans*-2-butene (27 %) and, during the summer campaign, isoprene (10 %), with O_3 reacting mainly

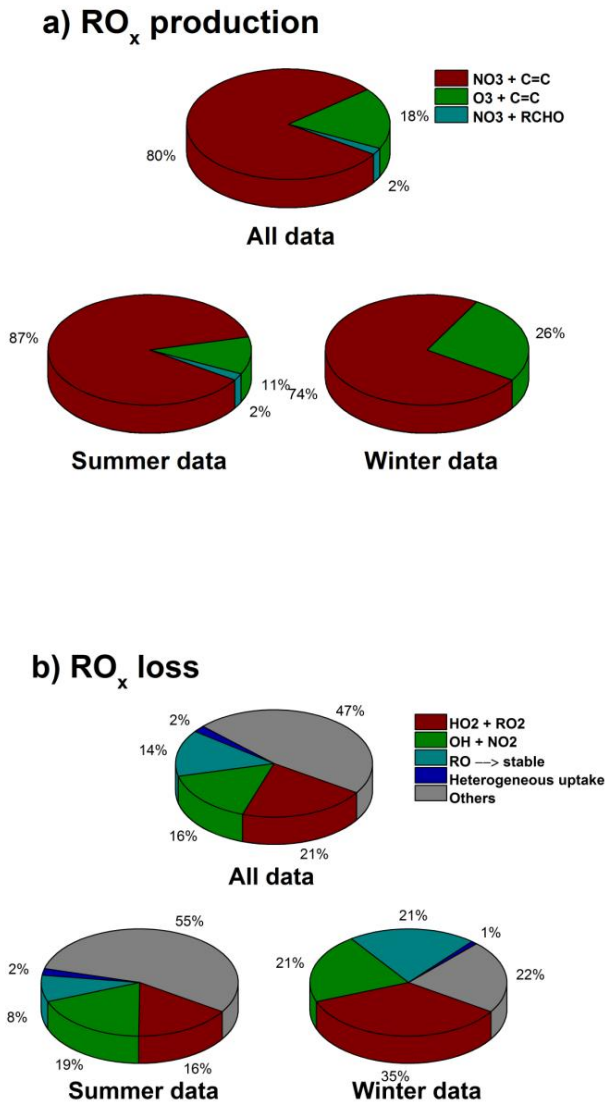

Fig. 7. Processes controlling the instantaneous production **(a)** and loss **(b)** of RO_x ($= RO + RO_2 + OH + HO_2$) radicals at night. The upper panels show the summer and winter campaign means combined, with the lower panels showing the summer campaign means (left hand side) and winter campaign means (right hand side). The average total production rate of RO_x was $(1.3 \pm 1.1) \times 10^5\,cm^{-3}\,s^{-1}$ (median $= 1.0 \times 10^5\,cm^{-3}\,s^{-1}$) for the entire data set, $(1.6 \pm 1.4) \times 10^5\,cm^{-3}\,s^{-1}$ (median $= 1.2 \times 10^5\,cm^{-3}\,s^{-1}$) for the summer campaign and $(1.0 \pm 0.4) \times 10^5\,cm^{-3}\,s^{-1}$ (median $= 0.9 \times 10^5\,cm^{-3}\,s^{-1}$) for the winter campaign. The average total loss rate of RO_x was $(1.6 \pm 1.2) \times 10^5\,cm^{-3}\,s^{-1}$ (median $= 1.2 \times 10^5\,cm^{-3}\,s^{-1}$) for the entire data set, $(1.9 \pm 1.4) \times 10^5\,cm^{-3}\,s^{-1}$ (median $= 1.6 \times 10^5\,cm^{-3}\,s^{-1}$) for the summer campaign and $(1.0 \pm 0.3) \times 10^5\,cm^{-3}\,s^{-1}$ (median $= 0.9 \times 10^5\,cm^{-3}\,s^{-1}$) for the winter campaign.

with *trans*-2-butene (51 %), propene (22 %), ethene (13 %) and *iso*-butene (5 %). Reactions of NO_3 with aldehydes also result in radical production at night, particularly during the winter campaign, with $NO_3 + HCHO$ contributing the greatest influence from aldehyde species.

Figure 7 shows that radical loss is controlled by a number of processes. Production of peroxides, through $RO_2 + HO_2$ and $HO_2 + HO_2$, represents 21 % of the RO_x radical loss, on average, followed by production of HNO_3 by $OH + NO_2$ (16 %), decomposition reactions of RO radicals to produce stable products (14 %) and heterogeneous losses (2 %). The large fraction of remaining loss processes (47 % of the total) is comprised largely of a myriad of $RONO_2$ and RO_2NO_2 production routes.

Overall, reactions of NO_3 with VOCs typically control the production of radicals during the campaign, with the unsaturated C_4 compounds dominating. There are a significant number of radical loss processes which produce organic nitrogen compounds, peroxides and nitric acid.

6.3 HO_x radical budgets

The processes controlling production and loss of nighttime HO_x ($HO_x = OH + HO_2$) radicals during RONOCO are shown in Fig. 9. Alkoxy radicals (RO), produced primarily following production of RO_2 from $NO_3 +$ alkene reactions and the subsequent reactions of RO_2 with NO_3, are a major source of HO_x, producing HO_2 through $RO + O_2$ reactions and on average representing 63 % of the total HO_x production. Specifically, the reaction of methoxy radicals (CH_3O) with O_2 dominates the HO_x production from RO radicals (31 % of the total HO_x production), with CH_3O primarily produced at night by $CH_3O_2 + NO_3$, and nighttime CH_3O_2 production primarily occurring through OH-initiated oxidation of CH_4 (48 %) and alkene ozonolysis reactions (37 %). Alkene ozonolysis reactions also produce OH and HO_2 radicals directly through the decomposition of Criegee intermediates, and are responsible for 20 % of the total HO_x production, although there is still much uncertainty regarding radical yields from ozonolysis reactions (Johnson and Marston, 2008). A further 17 % of HO_x radicals are generated as a result of direct HO_2 production by $NO_3 + HCHO$, using model calculated HCHO concentrations.

Reactions of HO_2 producing peroxides ($HO_2 + RO_2$ and $HO_2 + HO_2$) and formation of HNO_3 by the reaction of OH with NO_2 represent major sinks for HO_x radicals, comprising 23 and 25 % of the total loss, respectively. Heterogeneous loss of OH and HO_2, primarily through aerosol uptake of HO_2, represents 11 % of the total HO_x sink, and is more significant during winter (contributing 13 % to the total HO_x loss) compared to summer (contributing 4 % to the total HO_x loss). The remainder of HO_x loss occurs primarily through reactions of OH with VOCs, with $OH + CH_4$ alone constituting 19 % of the total HO_x sink.

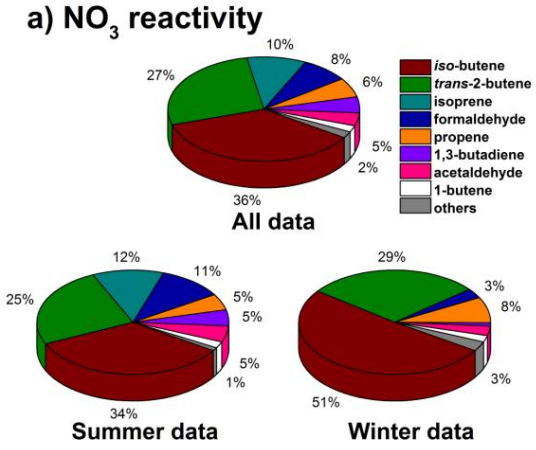

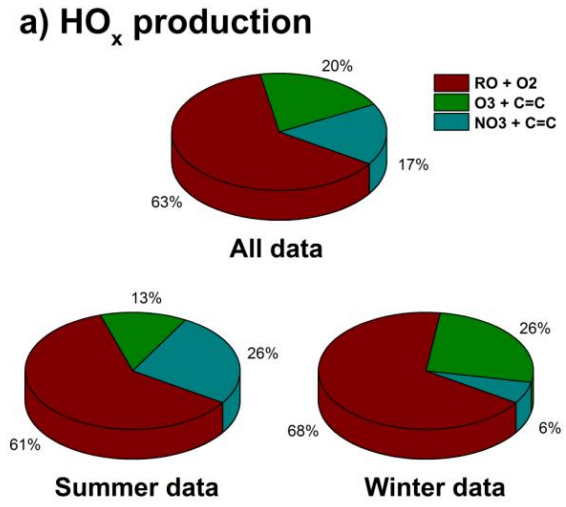

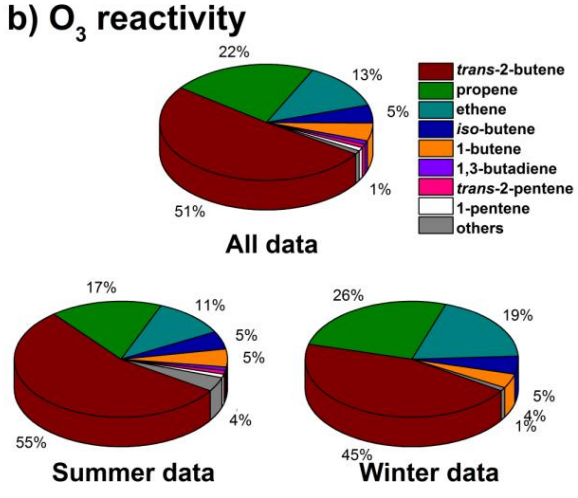

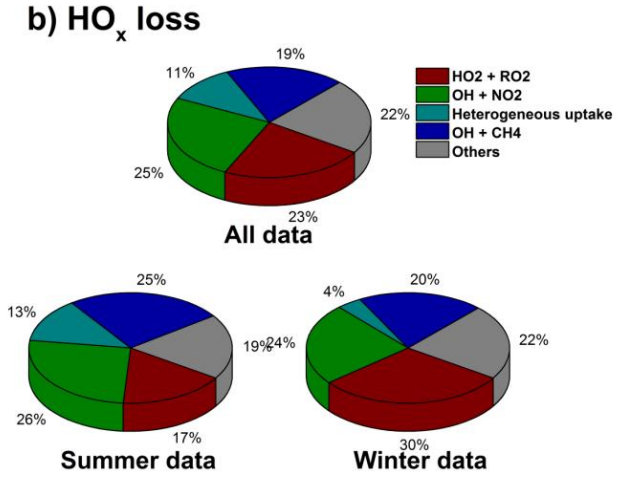

Fig. 8. Reactivity of **(a)** NO_3 and **(b)** O_3 towards observed VOCs at night during the RONOCO project. The upper panels show the summer and winter campaign means combined, with the lower panels showing the summer campaign means (left hand side) and winter campaign means (right hand side). The average NO_3 reactivity towards VOCs was $6.6 \times 10^4\,cm^{-3}\,s^{-1}$ (median $= 5.3 \times 10^4\,cm^{-3}\,s^{-1}$) for the entire data set, $6.8 \times 10^4\,cm^{-3}\,s^{-1}$ (median $= 4.6 \times 10^4\,cm^{-3}\,s^{-1}$) for the summer campaign and $6.2 \times 10^4\,cm^{-3}\,s^{-1}$ (median $= 6.0 \times 10^4\,cm^{-3}\,s^{-1}$) for the winter campaign. The average O_3 reactivity towards VOCs was $2.1 \times 10^4\,cm^{-3}\,s^{-1}$ (median $= 2.1 \times 10^4\,cm^{-3}\,s^{-1}$) for the entire data set, $1.8 \times 10^4\,cm^{-3}\,s^{-1}$ (median $= 1.7 \times 10^4\,cm^{-3}\,s^{-1}$) for the summer campaign and $2.9 \times 10^4\,cm^{-3}\,s^{-1}$ (median $= 2.6 \times 10^4\,cm^{-3}\,s^{-1}$) for the winter campaign.

Fig. 9. Processes controlling the instantaneous production **(a)** and loss **(b)** of HO_x (i.e. $OH + HO_2$) radicals at night. The upper panels show the summer and winter campaign means combined, with the lower panels showing the summer campaign means (left hand side) and winter campaign means (right hand side). The average total production rate of HO_x was $(6.7 \pm 4.7) \times 10^4\,cm^{-3}\,s^{-1}$ (median $= 5.7 \times 10^4\,cm^{-3}\,s^{-1}$) for the entire data set, $(7.4 \pm 5.7) \times 10^4\,cm^{-3}\,s^{-1}$ (median $= 5.7 \times 10^4\,cm^{-3}\,s^{-1}$) for the summer campaign and $(5.7 \pm 2.1) \times 10^4\,cm^{-3}\,s^{-1}$ (median $= 5.6 \times 10^4\,cm^{-3}\,s^{-1}$) for the winter campaign. The average total loss rate of HO_x was $(7.1 \pm 4.9) \times 10^4\,cm^{-3}\,s^{-1}$ (median $= 6.0 \times 10^4\,cm^{-3}\,s^{-1}$) for the entire data set, $(7.7 \pm 6.0) \times 10^4\,cm^{-3}\,s^{-1}$ (median $= 6.0 \times 10^4\,cm^{-3}\,s^{-1}$) for the summer campaign and $(6.0 \pm 2.2) \times 10^4\,cm^{-3}\,s^{-1}$ (median $= 5.9 \times 10^4\,cm^{-3}\,s^{-1}$) for the winter campaign.

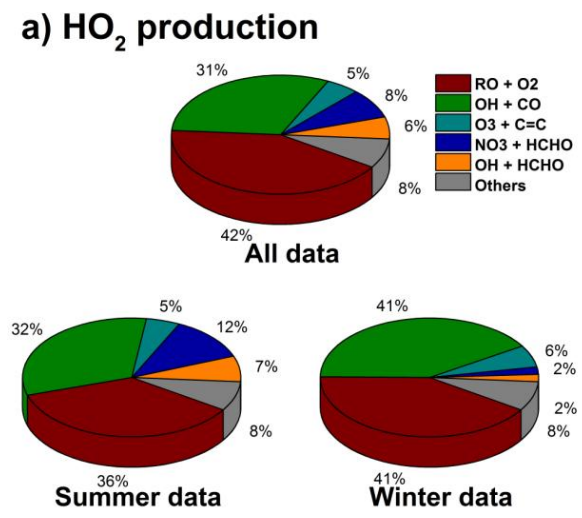

Fig. 10. Processes controlling the instantaneous production **(a)** and loss **(b)** of HO_2 radicals at night. The upper panels show the summer and winter campaign means combined, with the lower panels showing the summer campaign means (left hand side) and winter campaign means (right hand side). The average total production rate of HO_2 was $(9.3 \pm 5.6) \times 10^4$ cm^{-3} s^{-1} (median $= 7.9 \times 10^4$ cm^{-3} s^{-1}) for the entire data set, $(9.8 \pm 6.7) \times 10^4$ cm^{-3} s^{-1} (median $= 7.9 \times 10^4$ cm^{-3} s^{-1}) for the summer campaign and $(8.5 \pm 3.1) \times 10^4$ cm^{-3} s^{-1} (median $= 7.9 \times 10^4$ cm^{-3} s^{-1}) for the winter campaign. The average total loss rate of HO_2 was $(9.4 \pm 5.8) \times 10^4$ cm^{-3} s^{-1} (median $= 8.1 \times 10^4$ cm^{-3} s^{-1}) for the entire data set, $(9.9 \pm 7.0) \times 10^4$ cm^{-3} s^{-1} (median $= 8.0 \times 10^4$ cm^{-3} s^{-1}) for the summer campaign and $(8.8 \pm 3.2) \times 10^4$ cm^{-3} s^{-1} (median $= 8.2 \times 10^4$ cm^{-3} s^{-1}) for the winter campaign.

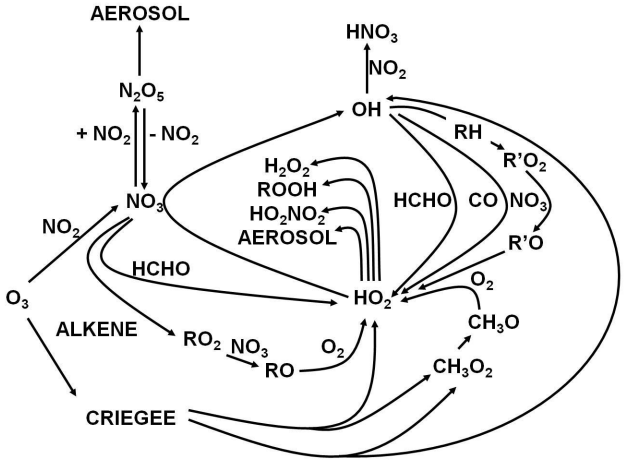

Fig. 11. Schematic summarising the dominant chemical pathways occurring during tropospheric oxidation at night during RONOCO.

Figure 10 shows the processes controlling modelled nighttime HO_2 concentrations during the campaign. Production of HO_2 is dominated by $RO + O_2$ reactions, comprising 42 % of the total on inclusion of $CH_3O + O_2$. Despite the low OH concentrations at night, there is also significant HO_2 production via $OH + CO$ (31 %). Alkene ozonolysis reactions represent 5 % of the total HO_2 production, on average, with reactions of HCHO with NO_3 and OH contributing 8 and 6 % to the total HO_2 production, respectively.

The dominant loss pathways for HO_2 are through reaction with NO_3 (45 % of the total) and O_3 (27 %), with both reactions representing radical propagation routes. Reactions of HO_2 with other peroxy radicals (both HO_2 and RO_2) constitute 17 % of the HO_2 loss, while uptake onto aerosols contributes only 7 % to the total HO_2 loss.

Production of OH at night occurred primarily through the reactions of HO_2 with NO_3 (53 %) and O_3 (33 %), with OH loss processes dominated by its reactions with CO (35 %), NO_2 (21 %), and CH_4 (12 %).

6.4 Summary of budget analyses

Figure 11 shows a summary of the processes controlling nighttime composition during RONOCO. In general we see a significant coupling between the NO_{3x} and RO_x families, with similar chemistry controlling the composition in summer and winter. The NO_{3x} family is primarily controlled by the balance between its production from the reaction of NO_2 and O_3 and its loss predominantly to aerosols through N_2O_5. However, the component of the loss not through this path (36 %, on average) is responsible for a dynamic organic chemistry. The reactions of NO_3 with alkenes, and of NO_3 with C_4-alkenes in particular, represent the dominant radical source at night during RONOCO, with radical losses owing to a combination of heterogeneous processes, peroxide formation (through $HO_2 + RO_2$ and $HO_2 + HO_2$),

decomposition of alkoxy radicals and formation of HNO_3 through the reaction of OH with NO_2. The propagation of the radical oxidation chemistry, which during the day would be controlled by NO is, at night, controlled by NO_3. Thus the NO_3 radical acts both as a chain initiator (like OH during the day) and the chain propagator (like NO during the day).

Production of HO_x radicals is typically dominated by reactions of RO radicals with O_2, with a minor contribution from alkene ozonolysis reactions. Loss of HO_x is largely controlled by $HO_2 + RO_2$ reactions and $OH + NO_2$, while the loss of HO_2 is typically dominated by the radical propagation reactions $HO_2 + NO_3$ and $HO_2 + O_3$.

Now that the chemistry occurring in the model during the night has been described, the model sensitivity to various uncertainties can be evaluated so that the reasons for the model's overprediction of NO_{3x} and underprediction of HO_2 can be investigated.

7 Sources of model uncertainties

Model calculations for RONOCO display a tendency to underpredict HO_2* whilst overpredicting NO_3 and N_2O_5. In this section we investigate the impact of potential sources of uncertainty on models of nighttime chemistry and composition. First we consider the impact of the timescale adopted in the model to describe physical losses of long-lived species in the model. Secondly, given the role of heterogenous uptake of N_2O_5 in determining NO_{3x} loss processes and the significant uncertainty in uptake coefficients in the literature (Brown et al., 2006, 2009, 2011; Escoreia et al., 2010; Tang et al., 2010; Badger et al., 2006; Thornton and Abbatt, 2005; Hallquist et al., 2003; Thornton et al., 2003; Kane et al., 2001; Hu and Abbatt, 1997; Fried et al., 1994; Van Doren et al., 1991; Hanson and Ravishankara, 1991; Mozurkewich and Calvert, 1998) we investigate the model sensitivity to $\gamma_{N_2O_5}$ and to the model description of heterogeneous uptake on aerosol surfaces. We then focus on model uncertainties which have the potential to rectify both the model underprediction of HO_2* and overprediction of NO_{3x}, i.e. parameters which are simultaneously sinks of NO_{3x} and sources of HO_x such as the reaction rate between NO_3 and RO_2 and the impact of missing VOCs.

7.1 Impact of timescale for physical loss

As described in Sect. 4, model calculations reported here include a first-order loss process to represent continuous physical loss processes to prevent the build-up of unmeasured species in the model. In our previous work as part of the African Monsoon Multidisciplinary Analyses (AMMA) campaign we investigated the impact of the rate of physical loss on HO_x simulations (Stone et al., 2010). Results of model simulations for daytime chemistry during AMMA indicated little impact of the physical loss rate on modelled

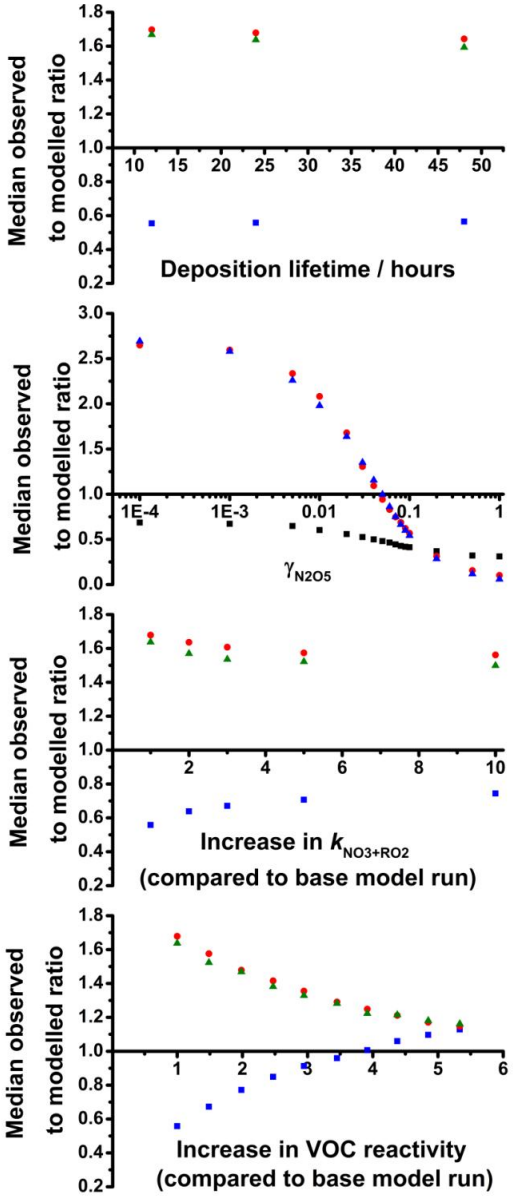

Fig. 12. Sensitivity of median modelled to observed ratios of HO_2* (blue), NO_3 (red) and N_2O_5 (green) towards **(a)** the deposition lifetime adopted in the model, **(b)** $\gamma_{N_2O_5}$, **(c)** rate coefficients for $NO_3 + RO_2$ ($k_{NO_3+RO_2}$) adopted in the model, and **(d)** concentrations of unsaturated VOCs in the model. Changes to $k_{NO_3+RO_2}$ and unsaturated VOC concentrations are represented as the factor by which $k_{NO_3+RO_2}$ and total unsaturated VOC concentration have been increased compared to the base run.

HO_2 concentrations, with the lifetimes with respect to physical loss varied between 1 h and 5 days (Stone et al., 2010). Figure 12a shows the impact of the modelled timescale for physical loss on the nighttime RONOCO simulations for HO_2 and NO_{3x}. There is little impact on modelled HO_2 or NO_{3x} on variation of the lifetime for physical loss from 12 to 48 h. Thus it does not seem likely that the simplistic

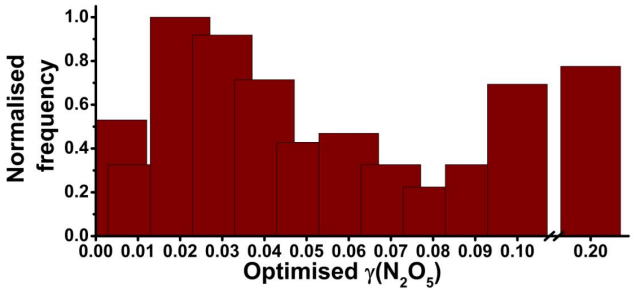

Fig. 13. Normalised probability distribution function for optimised values of $\gamma_{N_2O_5}$.

treatment of deposition or mixing processes considered in the model is able to explain the overall performance of the model.

7.2 Impact of $\gamma_{N_2O_5}$ and model descriptions of heterogeneous uptake on aerosols

Both laboratory and field studies of the value of $\gamma_{N_2O_5}$ are highly variable (Wagner et al., 2013; Riedel et al., 2012; Brown et al., 2011; Escoreia et al., 2010; Tang et al., 2010; Macintyre and Evans, 2010; Bertram and Thornton, 2009; Brown et al., 2006, 2009; Badger et al., 2006; Thornton and Abbatt, 2005; Hallquist et al., 2003; Thornton et al., 2003; Kane et al., 2001; Hu and Abbatt, 1997; Fried et al., 1994; Van Doren et al., 1991; Hanson and Ravishankara, 1991; Mozurkewich and Calvert, 1998) with values varying over an order of magnitude (10^{-4}–1). The base model uses a fixed value of $\gamma_{N_2O_5} = 0.02$, based on a global mean value (Evans and Jacob, 2005).

In order to investigate the sensitivity of the model we repeat all the simulations with a range of $\gamma_{N_2O_5}$ values (0, 1×10^{-6}, 1×10^{-5}, 1×10^{-4}, 1×10^{-3}, 5×10^{-3}, 0.01–0.1 (in 0.01 steps), 0.2, 0.5 and 1). For each model point we then select the value of gamma which gives the best fit between the modelled and observed concentrations of N_2O_5 (i.e. modelled to observed ratio closest to unity).

Figure 13 shows the normalised probability distribution function for the optimised values of $\gamma_{N_2O_5}$, indicating the greatest probability at $\gamma_{N_2O_5} = 0.02$ and a second peak in the probability distribution function at $\gamma_{N_2O_5} = 0.2$. The median value for the optimised $\gamma_{N_2O_5}$ is 0.05. The broad distribution of optimised values for $\gamma_{N_2O_5}$ observed in this work is supported by the large range of $\gamma_{N_2O_5}$ values reported in laboratory and field studies of N_2O_5 uptake, and highlights the difficulty in providing a full parameterisation of $\gamma_{N_2O_5}$ for use in atmospheric models.

Figure 14 shows the mean of the fractional aerosol composition (measured by the aerodyne mass spectrometer (AMS) onboard the BAe 146), temperature and humidity for data points within each optimised value for $\gamma_{N_2O_5}$. The optimised $\gamma_{N_2O_5}$ can be seen to display a general increase with increasing sulfate content of the aerosol, and with increasing sulfate to organic ratio, humidity and temperature, with $\gamma_{N_2O_5}$ increasing exponentially with each parameter. Despite the low chloride content of the aerosol, chloride reacts rapidly with dissolved N_2O_5 and can significantly affect the rate of N_2O_5 uptake even at low concentrations (Behnke et al., 1997; Bertram and Thornton, 2009; Roberts et al., 2009), with the optimised values for $\gamma_{N_2O_5}$ displaying an increase with the increasing chloride content of the aerosol. Decreases in the optimised values for $\gamma_{N_2O_5}$ are found with increasing nitrate fraction of the aerosol and ammonium to sulfate ratio, with smaller decreases observed with increasing ammonium and organic fractions. Such behaviour has been observed previously in a number of laboratory and field studies (see, for example, Brown et al., 2006; Bertram and Thornton, 2009; Chang et al., 2011; Brown and Stutz, 2012; Riedel et al., 2012, 2013; Wagner et al., 2013; Bertram et al., 2009; and Gaston et al., 2013), and optimisation of $\gamma_{N_2O_5}$ through use of model simulations to reach agreement between ambient gas phase measured and modelled N_2O_5 has been reported in previous work (Wagner et al., 2013).

However, while optimisation of $\gamma_{N_2O_5}$, by definition, gives model success for NO_3 and N_2O_5, the modelled concentrations of HO_2 are not improved by optimising $\gamma_{N_2O_5}$, with the median modelled to observed ratio for HO_2* decreasing from 0.56 for the base model run ($\gamma_{N_2O_5} = 0.02$) to 0.52 for the model run using optimised values for $\gamma_{N_2O_5}$. The optimised values for $\gamma_{N_2O_5}$ result in lower modelled HO_2 concentrations since the lower concentrations of NO_{3x} lead to decreased rates of radical production from NO_3-initiated oxidation processes. Thus, although there are large uncertainties associated with $\gamma_{N_2O_5}$, and evidence for a dependence of $\gamma_{N_2O_5}$ on aerosol composition, humidity and temperature, the uncertainties in $\gamma_{N_2O_5}$ cannot fully explain the model uncertainty observed during RONOCO.

While a range of aerosol uptake coefficients for HO_2 have been reported in the literature (see, for example, George et al., 2013), heterogeneous uptake of HO_2 was found to constitute a relatively minor loss process for HO_2 (7 % of the total) and RO_x radicals (< 2 % of the total), as discussed in Sect. 6. There is thus little model sensitivity to γ_{HO_2}.

We now investigate model sensitivity to other parameters in the model which are able to simultaneously reduce the modelled concentrations of NO_{3x} whilst also increasing the modelled concentrations of HO_2.

7.3 Impact of $k_{NO_3+RO_2}$

The reaction between peroxy (RO_2) radicals and NO_3 are central for the production of HO_2 at night and play an important role in removing NO_3. There have been, however, very few studies of this important class of compounds (see for example Vaughan et al., 2006) compared to equivalent studies of daytime radical reactions. The MCM considers three different reactions rates for this class, one for CH_3O_2, one for

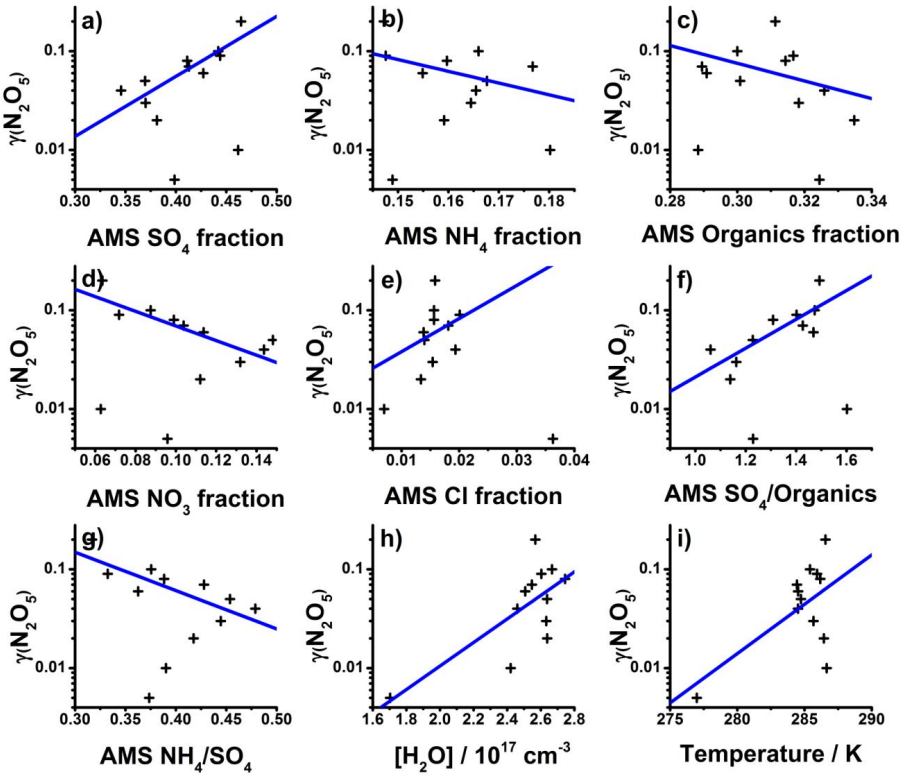

Fig. 14. Relationships between the optimised values for $\gamma_{N_2O_5}$ and the corresponding **(a)** fractional contribution of sulfate aerosol to the total aerosol mass, **(b)** fractional contribution of ammonium aerosol to the total aerosol mass, **(c)** fractional contribution of organic aerosol to the total aerosol mass, **(d)** fractional contribution of nitrate aerosol to the total aerosol mass, **(e)** fractional contribution of chloride aerosol to the total aerosol mass, **(f)** ratio of sulfate aerosol mass to organic aerosol mass, **(g)** ratio of ammonium aerosol mass to sulfate aerosol mass, **(h)** water vapour concentration, and **(i)** temperature. The best fit lines are shown in blue, and are described by **(a)** $y = 1.8 \times 10^{-3}\exp(7.8x)$, **(b)** $y = 0.8\exp(-18.2x)$, **(c)** $y = 4.2\exp(-14.8x)$, **(d)** $y = 6.3 \times 10^{-2}\exp(-3.8x)$, **(e)** $y = 9.9 \times 10^{-2}\exp(-49.5x)$, **(f)** $y = 4.3 \times 10^{-3}\exp(1.7x)$, **(g)** $y = 0.5\exp(-6.0x)$, **(h)** $y = 4.4 \times 10^{-5}\exp(2.7\times 10^{-17}x)$, and **(i)** $y = 1.6 \times 10^{-30}\exp(0.2x)$.

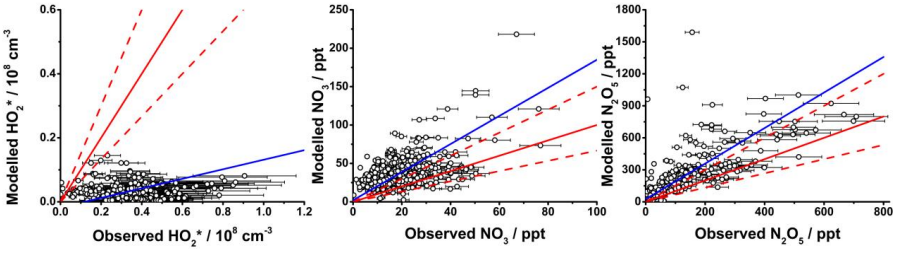

Fig. 15. Comparison between modelled and observed concentrations of **(a)** HO_2*, **(b)** NO_3 and **(c)** N_2O_5 for a model run including summer and winter data in which alkene concentrations are set to zero. In each plot, the solid red line indicates the 1 : 1 line, with 50 % limits given by the broken red lines. The best fit lines are shown in blue, and are described by $[HO_2^*]_{mod} = \{(0.2 \pm 0.1) \times [HO_2^*]_{obs}\} - (1.8 \pm 2.6) \times 10^6$ cm^{-3} ($r^2 < 0.01$), $[NO_3]_{mod} = \{(1.8 \pm 0.2) \times [NO_3]_{obs}\} + (2.1 \pm 3.8)$ ppt ($r^2 = 0.3$) and $[N_2O_5]_{mod} = \{(1.6 \pm 0.1) \times [N_2O_5]_{mod}\} - (39.2 \pm 22.2)$ ppt ($r^2 = 0.6$). Errors bars are 1σ.

$RC(O)O_2$ and one for all other RO_2, with no temperature dependence considered and all reaction products assumed to be analogous to the corresponding reaction of the RO_2 radical with NO.

Figure 12c shows the sensitivity of the mean modelled to observed ratios of HO_2 and NO_{3x} on $k_{NO_3+RO_2}$, where all $k_{NO_3+RO_2}$ have been increased by the same factor. We find that increases in $k_{NO_3+RO_2}$ lead to increases in modelled HO_2* and decreases in modelled NO_{3x}, but large (> 10) changes in $k_{NO_3+RO_2}$ are required to significantly improve the model success. However, there have been no measurements of the kinetics of peroxy radicals derived from NO_3-

initiated oxidation, which are significant at night, and there may be significant differences in the behaviour of peroxy radicals derived from OH- and O_3-initiated oxidation, which are used to estimate $k_{NO_3+RO_2}$ in the model, and those derived from NO_3-initiated oxidation. The presence of unknown VOCs (Sect. 7.4), and thus of unknown RO_2 radicals, leads to further uncertainties in $k_{NO_3+RO_2}$. The available database of laboratory data concerning radical processing in nighttime atmospheres is extremely limited.

7.4 Impact of VOC concentrations

Reactions of NO_3 with VOCs are important for both NO_3 loss and RO_x radical production. Previous studies have invoked unmeasured VOCs to explain both model overpredictions of NO_3 and underpredictions of HO_2.

The presence of unmeasured unsaturated VOCs also leads to uncertainty in the model. Figure 15 displays the comparison between modelled and observed concentrations of HO_2, NO_3 and N_2O_5 for a model run in which the concentrations of all species containing C=C were set to zero. Compared to the base model run (Fig. 2), the run with no unsaturated hydrocarbons shows a marked increase in modelled concentrations of NO_{3x} and very little HO_2 production, demonstrating the significance of unsaturated VOCs as both a sink of NO_{3x} and a source of HO_2. The presence of unquantified or unmeasured VOCs thus has the potential to improve model simulations for both HO_2 and NO_{3x}.

Figure 12d shows the impact of increasing the concentration of unsaturated VOCs on the mean modelled to measured ratios of HO_2, NO_3 and N_2O_5, represented as the increase in reactivity towards NO_3, where the reactivity is given by $\Sigma k_{NO_3+VOC}[VOC]$. An increase of approximately 4 times the total observed C=C reactivity results in significant improvements to model simulations for HO_2*, and simultaneously improves the modelled NO_{3x}. The percentage interferences in HO_2* owing to alkene-derived RO_2 radicals are similar for the base model run (17.0 %) and the model run with increased C=C reactivity (16.8 %).

Thus significant concentrations of unmeasured VOCs during RONOCO may explain the model measurement discrepancy. Previous work using two-dimensional gas chromatography (2-D-GC) in urban environments isolated and classified over 500 different VOCs not routinely measured, with significant impacts on atmospheric chemistry (Lewis et al., 2000). 2-D-GC analyses of the whole air samples (WAS) collected during the RONOCO campaign have also revealed the presence of a large number of VOCs which are not routinely measured (Lidster et al., 2013). Although the 2-D-GC analyses identify the presence of additional species, and, based on expected relationships between polarity and boiling point, can identify the presence of additional unsaturated VOCs, the current absence of readily available calibration standards for long-chain alkenes and other unsaturated VOCs makes full identification and quantification of such species impractical.

Biogenic compounds such as monoterpenes have the potential to significantly impact on the nighttime chemistry. A model run in which α-pinene was included at a concentration equivalent to the limit of detection (131–280 ppt) for the proton transfer mass spectrometer (PTR-MS) onboard the BAe 146 during RONOCO, decreased the median modelled to observed ratios for NO_3 and N_2O_5 from 1.68 and 1.64, respectively, for the base model run to 0.76 and 0.82, respectively. Thus total monoterpenes in the 100 ppt range would significantly improve the fidelity of the NO_3 and N_2O_5 simulation. However, the median modelled to observed ratio for HO_2* was reduced from 0.56 for the base model run to 0.34 on inclusion of α-pinene. This reduction is predominantly due to α-pinene derived RO radicals undergoing internal rearrangements to produce carbonyl compounds and NO_2, in preference to reaction with O_2 to produce carbonyl compounds and HO_2 as exhibited by other unsaturated VOCs. Similarly, inclusion of styrene in the model at concentrations equivalent to those observed for ethylbenzene (median $\sim$ 8 ppt) reduced the median modelled to observed ratios for NO_3 and N_2O_5 to 1.31 and 1.11, respectively, but also reduced the median modelled to observed ratio for HO_2* to 0.29 owing to similar behaviour of styrene-derived RO_2 radicals to those derived from monoterpenes. Low concentrations of species such as monoterpenes and styrene which display high reactivity towards NO_3 can thus have a significant impact on NO_{3x} concentrations, and the presence of such compounds may reduce the N_2O_5 aerosol uptake coefficient required to achieve model success for NO_{3x}, but the larger hydrocarbons appear to be less efficient at generating HO_2 and cannot fully explain the model discrepancies observed for this work.

Other biogenic compounds such as dimethyl sulfide (DMS) have the potential to impact the nighttime radical chemistry. DMS is a potential sink for NO_3 and source of RO_x radicals, with previous measurements at ground level in marine and coastal regions showing DMS to be a significant sink for NO_3 (Carslaw et al., 1997; Allan et al., 1999). DMS concentrations reported over the North Sea and at the Weybourne Atmospheric Observatory on the North Sea coast have indicated high variability at ground level, varying from <10 to over 300 ppt (Allan et al., 1999; Burgermeister and Georgii, 1991; Carslaw et al., 1997) and typically decreasing rapidly with altitude (Blake et al., 1999; Lunden et al., 2010; Spicer et al., 1996; Andreae et al., 1985). However, DMS was not observed above its 3 ppt limit of detection during the RONOCO campaign. A model run including 3 ppt of DMS did result in improved model success for HO_2* and NO_{3x}, increasing the median modelled to observed ratio for HO_2* from 0.56 for the base model run to 0.68 for the model run including 3 ppt DMS and decreasing the median modelled ratios for NO_3 and N_2O_5 from 1.68 and 1.64 to 1.36 and 1.39, respectively. The improvements were thus not sufficient to fully explain the discrepancies.

We thus conclude that unquantified species containing C=C could reconcile model and measured NO_3, N_2O_5 and

HO_2. However, their exact nature remains unknown. Any compound would have to be heavy enough to not be measured using the GC-FID system yet small enough not to exhibit the tendency for radical internal rearrangement which limits the ability to produce HO_2.

8 Future studies

The RONOCO data set is one of the few data sets that has made extensive nighttime observations of both HO_x and NO_{3x}, particularly in regions with significant NO_x concentrations but remote from primary sources. There is a paucity of previous studies of these chemical regimes leading to uncertainty about the chemistry occurring in such chemical systems. The uncertainties found in this study could be reduced by providing direct observations of higher alkenes and terpenes at low levels. Given the high modelled RO_2 to HO_2 ratios, a measurement of RO_2 concentrations would provide a significant constraint on the chemistry. The N_2O_5 uptake coefficient has been shown to display a complex dependence on aerosol composition, humidity and temperature (see for example, Brown et al., 2006; Bertram and Thornton, 2009; Brown and Stutz, 2012; Riedel et al., 2012; Wagner et al., 2013; Gaston et al., 2013), and further laboratory studies of $\gamma_{N_2O_5}$ leading to improved parameterisations of these effects would significantly reduce the model uncertainty. Measurements of $RO_2 + NO_3$ rate coefficients for a variety of RO_2 radicals and under a range of temperatures and pressures would also improve our understanding of this system.

9 Conclusions

Nighttime measurements of HO_2*, NO_3 and N_2O_5 over the UK during the RONOCO project have been compared to box model calculation simulations using the MCM. The model tends to underestimate HO_2*, whilst overestimating NO_3 and N_2O_5. We find that $NO_3 + VOC$ chemistry is the most significant source of RO_x radicals in the model, and that reactions of NO_3 with peroxy radicals dominate radical propagation. We observe a strong coupling between HO_2 and NO_3 at night, in both the measurements and the model calculations, although there are significant uncertainties associated with modelling of nighttime oxidation chemistry. Model simulations for NO_3 and N_2O_5 can be improved through the use of increased aerosol uptake coefficients for N_2O_5, with optimised values for N_2O_5 uptake coefficients increasing with sulfate aerosol content, humidity and temperature. However, the improvements for NO_3 and N_2O_5 achieved through optimisation of the uptake coefficient for N_2O_5 are at the expense of model success for HO_2. Improvements to model simulations for HO_2, NO_3 and N_2O_5 can be achieved through the inclusion of additional unsaturated VOCs in the model. However, these missing VOCs would have to be in significant concentrations and have a significant HO_2 yield. We conclude that the inclusion of appropriate $NO_3 + VOC$ and $NO_3 + RO_2$ chemistry is essential to successful model simulations of tropospheric oxidation at night.

Appendix A

Model treatment of potential RO_2 interferences in HO_2 measurements

Following the work of Fuchs et al. (2011), the Leeds aircraft FAGE instrument was investigated for potential interferences in measurements of HO_2 from alkene-derived RO_2 radicals. Experimental conditions are discussed in detail by Whalley et al. (2013), and are provided only briefly here. Interference testing was conducted using the FAGE calibration setup described by Commane et al. (2010), in which equal amounts of OH and HO_2 are produced by passing a known flow ($\sim 50\,dm^3\,min^{-1}$) of humidified ultra-high purity air (BTCA 178, BOC Special Gases) across a low pressure mercury lamp of known actinic flux:

$$H_2O + h\nu(\lambda = 184.9\,nm) \rightarrow H + OH,$$

$$H + O_2 + M \rightarrow HO_2 + M.$$

In order to generate RO_2 radicals in the flow an excess of the parent hydrocarbon was added to the flow, such that the OH radicals produced were converted stoichiometrically to RO_2, resulting in equal amounts of HO_2 and RO_2 in the flow:

$$OH + RH \rightarrow R + H_2O,$$

$$R + O_2 + M \rightarrow RO_2 + M.$$

Comparison of observed signals in the HO_2 detection cell with and without addition of the parent hydrocarbon thus enables determination of the RO_2 interference. For this work, interferences were investigated for RO_2 radicals derived from ethene giving an interference of $(39.7 \pm 4.8)\,\%$ for 1:1 $HO_2 : RO_2$ mixtures.

The chemistry responsible for producing RO_2 interferences in HO_2 measurements by FAGE appears to be well described by the MCM (Fuchs et al., 2011; Whalley et al., 2013), and the total potential interference in the measurements made during RONOCO were thus estimated with an MCM based box model. The box model, constrained to the characteristics of the FAGE instrument (cell pressure of 1.8 Torr; cell temperature of 260 K; NO concentration $\sim 10^{14}\,cm^{-3}$) and initialised with equal amounts of HO_2 and all organic RO_2 radicals described in the MCM was run forwards in time until the modelled interferences from RO_2 radicals derived from ethene reached the experimentally derived values of 40 %. An interference factor, f, was then determined from the model output for each RO_2 radical, where f is the fractional change in the modelled HO_2 signal (i.e. the amount of OH produced) for a 1 : 1 mixture of HO_2

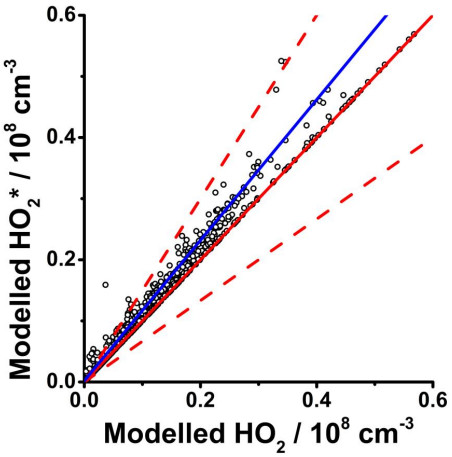

Fig. A1. Comparison between modelled HO_2* (the sum of HO_2 and potential RO_2 interferences) and modelled HO_2 for RONOCO. The solid red line indicates the 1:1 line, with 50 % limits given by the broken red lines. The best fit line is shown in blue and is described by $HO_2^* = [1.15 \times HO_2] + 2 \times 10^5$ cm^{-3}.

and RO_2. The modelled HO_2* (the combination of HO_2 and potential interferences from RO_2) was subsequently determined for each time point using $HO_2^* = HO_2 + fRO_2$ for direct comparison with the FAGE measurements. Figure A1 shows the comparison between modelled HO_2* and HO_2 for RONOCO, indicating that interferences during the campaign were generally small.

Acknowledgements. This work was funded by the UK Natural Environment Research Council (NE/F004664/1). The authors would like to thank ground staff, engineers, scientists and pilots involved in RONOCO for making this project a success. Airborne data were obtained using the BAe 146-301 Atmospheric Research Aircraft (ARA) flown by Directflight Ltd. and managed by the Facility for Airborne Atmospheric Measurements (FAAM), which is a joint entity of the Natural Environment Research Council (NERC) and the Met Office.

Edited by: J. Thornton

References

Aldener, M., Brown, S. S., Stark, H., Williams, E. J., Lerner, B. M., Kuster, W. C., Goldan, P. D., Quinn, P. K., Bates, T. S., Fehsenfeld, F. C., and Ravishankara, A. R.: Reactivity and loss mechanisms of NO_3 and N_2O_5 in a polluted marine environment: Results from in situ measurements during New England Air Quality Study 2002, J. Geophys. Res., 111, D23S73, doi:10.1029/2006JD007252, 2006.

Aliwell, S. R. and Jones, R. L.: Measurements of tropospheric NO_3 at midlatitude, J. Geophys. Res. Atmos., 103, 5719–5727, 1998.

Allan, B. J., Carslaw, N., Coe, H., Burgess, R. A., Plane, J. M. C.: Observations of the nitrate radical in the marine boundary layer, J. Atmos. Chem., 33, 129–154, 1999.

Allan, B. J., Plane, J. M. C., Coe, H., Shillto, J.: Observations of NO_3 concentration profiles in the troposphere, J. Geophys. Res., 107, 4588, doi:10.1029/2002JD002112, 2002.

Andreae, M. O., Ferek, R. J., Bermond, F., Byrd, K. P., Engstrom R. T., Hardin, S., Houmere, P. D., LeMarrec, F., and Raemdonck, H.: Dimethyl sulfide in the marine atmosphere, J. Geophys. Res., 90, 12891–12900, 1985.

Badger, C. L., Griffiths, P. T., George, I., Abbattt, J. P. D., and Cox, R. A.: Reactive Uptake of N_2O_5 by Aerosol Particles Containing Mixtures of Humic Acid and Ammonium Sulfate, J. Phys. Chem. A., 110, 6986–6994, 2006.

Behnke, W., George, C., Scheer, V., and Zetzsch, C.: Production and decay of $ClNO_2$ from the reaction of gaseous N_2O_5 with NaCl solution: Bulk and aerosol experiments, J. Geophys. Res. Atmos., 102, 3795–3804, doi:10.1029/96JD03057, 1997.

Bertram, T. H. and Thornton, J. A.: Toward a general parameterization of N_2O_5 reactivity on aqueous particles: the competing effects of particle liquid water, nitrate and chloride, Atmos. Chem. Phys., 9, 8351–8363, doi:10.5194/acp-9-8351-2009, 2009.

Bertram, T. H., Thornton, J. A., Riedel, T. P., Middlebrook, A. M., Bahreini, R., Bates, T. S., Quinn, P. K., and Coffman, D. J.: Direct observations of N_2O_5 reactivity on ambient aerosol particles, Geophys. Res. Lett., 36, L19803, doi:10.1029/2009GL040248, 2009.

Blake, N. J., Blake, D. R., Wingenter, O. W., Sive, B. C., Kang, C. H., Thornton, D. C., Bandy, A. R., Atlas, E., Flocke, F., Harris, J. M., and Sherwood Rowland, F.: Aircraft measurements of the latitudinal, vertical and seasonal variations of NMHCs, methyl nitrate, methyl halides, and DMS during the First Aerosol Characterization Experiment (ACE 1), J. Geophys. Res., 104, 21803–21817, 1999.

Bloss, W. J., Gravestock, T. J., Heard, D. E., Ingham, T., Johnson, G. P., and Lee, J. D.: Application of a compact all solid-state laser system to the in situ detection of atmospheric OH, HO_2, NO and IO by laser-induced fluorescence, J. Environ. Monit., 5, 21–28, 2003.

Brough, N., Reeves, C. E., Penkett, S. A., Stewart, D. J., Dewey, K., Kent, J., Barjat, H., Monks, P. S., Ziereis, H., Stock, P., Huntrieser, H., and Schlager, H.: Intercomparison of aircraft instruments on board the C-130 and Falcon 20 over southern Germany during EXPORT 2000, Atmos. Chem. Phys., 3, 2127–2138, doi:10.5194/acp-3-2127-2003, 2003.

Brown, S. S. and Stutz, J.: Nighttime radical observations and chemistry, Chem. Soc. Rev., 41, 6405–6447, 2012.

Brown, S. S., Stark, H., and Ravishankara, A. R.: Applicability of the steady state approximation to the interpretation of atmospheric observations of NO_3 and N_2O_5, J. Geophys. Res., 108, 4539, doi:10.1029/2003JD003407, 2003.

Brown, S. S., Dibb, J. E., Stark, H., Aldener, M., Vozella, M., Whitlow, S., Williams, E. J., Lerner, B. M., Jakoubek, R., Middlebrook, A. M., DeGouw, J. A., Warneke, C., Goldan, P. D., Kuster, W. C., Angevine, W. M., Sueper, D. T., Quinn, P. K., Bates, T. S., Meagher, J. F., Fehsenfeld, F. C., and Ravishankara, A. R.: Nighttime removal of NO_x in the summer marine boundary layer, Geophys. Res. Lett., 31, L07108, doi:10.1029/2004GL019412, 2004.

Brown, S. S., Ryerson, T. B., Wollny, A. G., Brock, C. A., Peltier, R., Sullivan, A. P., Weber, R. J., Dube, W. P., Trainer, M., Meagher, J. F., Fehsenfeld, F. C., and Ravishankara, A. R.: Vari-

ability in Nocturnal Nitrogen Oxide Processing and Its Role in Regional Air Quality, Science, 311, 67–70, 2006.

Brown, S. S., Dubé, W. P., Osthoff, H. D., Wolfe, D. E., Angevine, W. M., and Ravishankara, A. R.: High resolution vertical distributions of NO_3 and N_2O_5 through the nocturnal boundary layer, Atmos. Chem. Phys., 7, 139–149, doi:10.5194/acp-7-139-2007, 2007.

Brown, S. S., deGouw, J. A., Warneke, C., Ryerson, T. B., Dubé, W. P., Atlas, E., Weber, R. J., Peltier, R. E., Neuman, J. A., Roberts, J. M., Swanson, A., Flocke, F., McKeen, S. A., Brioude, J., Sommariva, R., Trainer, M., Fehsenfeld, F. C., and Ravishankara, A. R.: Nocturnal isoprene oxidation over the Northeast United States in summer and its impact on reactive nitrogen partitioning and secondary organic aerosol, Atmos. Chem. Phys., 9, 3027–3042, doi:10.5194/acp-9-3027-2009, 2009.

Brown, S. S., Dube, W. P., Peischl, J., Ryerson, T. B., Atlas, E., Warneke, C., de Gouw, J. A., Hekkert, S. t. L., Brock, C. A., Flocke, F., Trainer, M., Parrish, D. D., Fehsenfeld, F. C., and Ravishankara, A. R.: Budgets for nocturnal VOC oxidation by nitrate radicals aloft during the 2006 Texas Air Quality Study, J. Geophys. Res., 116, D24305, doi:10.1029/2011JD016544, 2011.

Burgermeister, S. and Georgii, H.-W.: Distribution of methanesulfonate, NSS sulfate and dimethylsulfide over the Atlantic and the North Sea, Atmos. Environ., Part A, 25, 587–595, 1991.

Carslaw, N., Carpenter, L. J., Plane, J. M. C., Allan, B. J., Burgess, R. A., Clemitshaw, K. C., Coe, H., and Penkett, S. A.: Simultaneous observations of nitrate and peroxy radicals in the marine boundary layer, J. Geophys. Res., 102, 18917–18933, 1997.

Chang, W. L. P., Bhave, P. V., Brown, S. S., Riemer, N., Stutz, J., and Dabdub, D.: Heterogeneous atmospheric chemistry, ambient measurements, and model calculations of N_2O_5: A review, Aerosol Sci. Technol., 45, 665–695, 2011.

Coe, H., Allan, J. D., Alfarra, M. R., Bower, K. N., Flynn, M. J., McFiggans, G. B., Topping, D. O., Williams, P. I., O'Dowd, C. D., Dall'Osto, M., Beddows, D. C. S., and Harrison, R. M.: Chemical and physical characteristics of aerosol particles at a remote coastal location, Mace Head, Ireland, during NAMBLEX, Atmos. Chem. Phys., 6, 3289–3301, doi:10.5194/acp-6-3289-2006, 2006.

Commane, R., Floquet, C. F. A., Ingham, T., Stone, D., Evans, M. J., and Heard, D. E.: Observations of OH and HO_2 radicals over West Africa, Atmos. Chem. Phys., 10, 8783–8801, doi:10.5194/acp-10-8783-2010, 2010.

Dari-Salisburgo, C., Di Carlo, P., Giammaria, F., Kajii, Y., and D'Altorio, A.: Laser induced fluorescence instrument for NO_2 measurements: observations at a central Italy background site, Atmos. Environ., 43, 970–977, 2009.

Di Carlo, P., Aruffo, E., Busilacchio, M., Giammaria, F., Dari-Salisburgo, C., Biancofiore, F., Visconti, G., Lee, J., Moller, S., Reeves, C. E., Bauguitte, S., Forster, G., Jones, R. L., and Ouyang, B.: Aircraft based four-channel thermal dissociation laser induced fluorescence instrument for simultaneous measurements of NO_2, total peroxy nitrate, total alkyl nitrate, and HNO3, Atmos. Meas. Tech., 6, 971–980, doi:10.5194/amt-6-971-2013, 2013.

Ehhalt, D. H. and Rohrer, F.: The tropospheric cycle of H_2: a critical review, Tellus, 61B, 500–535, 2009.

Emmerson, K. M. and Carslaw, N.: Night-time radical chemistry during the TORCH campaign, Atmos. Environ., 43, 3220–3226, 2009.

Emmerson, K. M. and Evans, M. J.: Comparison of tropospheric gas-phase chemistry schemes for use within global models, Atmos. Chem. Phys., 9, 1831–1845, doi:10.5194/acp-9-1831-2009, 2009.

Escoreia, E. N., Sjostedt, S. J., and Abbattt, J. P. D.: Kinetics of N_2O_5 Hydrolysis on Secondary Organic Aerosol and Mixed Ammonium Bisulfate-Secondary Organic Aerosol Particles, J. Phys. Chem. A, 114, 13113–13121, 2010.

Evans, M. J. and Jacob, D. J.: Impact of new laboratory studies of N_2O_5 hydrolysis on global model budgets of tropospheric nitrogen oxides, ozone, and OH, Geophys. Res. Lett., 32, 1–4, 2005.

Faloona, I., Tan, D., Brune, W., Hurst, J., Barket, D., Couch, T. L., Shepson, P., Apel, E., Riemer, D., Thornberry, T., Carroll, M. A., Sillman, S., Keeler, G. J., Sagady, J., Hooper, D., and Paterson, K.: Nighttime observations of anomalously high levels of hydroxyl radicals above a deciduous forest canopy, J. Geophys. Res. Atmos., 106, 24315–24333, 2001.

Fleming, Z. L., Monks, P. S., Rickard, A. R., Heard, D. E., Bloss, W. J., Seakins, P. W., Still, T. J., Sommariva, R., Pilling, M. J., Morgan, R., Green, T. J., Brough, N., Mills, G. P., Penkett, S. A., Lewis, A. C., Lee, J. D., Saiz-Lopez, A., and Plane, J. M. C.: Peroxy radical chemistry and the control of ozone photochemistry at Mace Head, Ireland during the summer of 2002, Atmos. Chem. Phys., 6, 2193–2214, doi:10.5194/acp-6-2193-2006, 2006.

Fried, A., Henry, B. E., Calvert, J. G., and Mozurkewich, M.: The reaction probability of N_2O_5 with sulfuric acid aerosols probed by the heterogeneous hydrolysis of N_2O_5, Geophys. Res. Lett., 99, 3517–3532, 1994.

Fuchs, H., Bohn, B., Hofzumahaus, A., Holland, F., Lu, K. D., Nehr, S., Rohrer, F., and Wahner, A.: Detection of HO_2 by laser-induced fluorescence: calibration and interferences from RO_2 radicals, Atmos. Meas. Tech., 4, 1209–1225, doi:10.5194/amt-4-1209-2011, 2011.

Gaston, C. J., Thornton, J. A., and Ng, N. L.: Reactive uptake of N_2O_5 to internally mixed inorganic and organic particles: the role of organic carbon oxidation state and inferred organic phase separations, Atmos. Chem. Phys. Discuss., 13, 32053–32092, doi:10.5194/acpd-13-32053-2013, 2013.

George, I. J., Matthews, P. S. J., Whalley, L. K., Brooks, B., Goddard, A., Baeza-Romero, M. T., and Heard, D. E.: Measurements of uptake coefficients for heterogeneous loss of HO_2 onto submicron inorganic salt aerosols, Phys. Chem. Chem. Phys., 15, 12829–12845, 2013.

Gerbig, C., Schmitgen, S., Kley, D., Volz-Thomas, A., Dewey, K., and Haaks, D.: An improved fast-response vacuum UV resonance fluorescence CO instrument, J. Geophys. Res. Atmos., 104, 1699–1704, 1999.

Geyer, A., Bachmann, K., Hofzumahaus, A., Holland, F., Konrad, S., Klupfel, T., Patz, H.-W., Perner, D., Mihelcic, D., Schafer, H.-J., Volz-Thomas, A., and Platt, U.: Nighttime formation of peroxy and hydroxyl radicals during the BERLIOZ campaign: Observations and modeling studies, J. Geophys. Res., 108, 8249, doi:10.1029/2001JD000656, 2003.

Hallquist, M., Stewart, D. J., Stephenson, S. K., and Cox, R. A.: Hydrolysis of N_2O_5 on sub-micron sulfate aerosols, Phys. Chem. Chem. Phys., 5, 3453–3463, 2003.

Hanson, D. R. and Ravishankara, A. R.: The reaction probabilities of $ClONO_2$ and N_2O_5 on 40 to 75 % sulfuric acid solutions, J. Geophys. Res., 96, 17307–17314, 1991.

Heard, D. E. and Pilling, M. J.: Measurement of OH and HO_2 in the troposphere, Chem. Rev., 103, 5163–5198, 2003.

Hewitt, C. N., Lee, J. D., MacKenzie, A. R., Barkley, M. P., Carslaw, N., Carver, G. D., Chappell, N. A., Coe, H., Collier, C., Commane, R., Davies, F., Davison, B., DiCarlo, P., Di Marco, C. F., Dorsey, J. R., Edwards, P. M., Evans, M. J., Fowler, D., Furneaux, K. L., Gallagher, M., Guenther, A., Heard, D. E., Helfter, C., Hopkins, J., Ingham, T., Irwin, M., Jones, C., Karunaharan, A., Langford, B., Lewis, A. C., Lim, S. F., MacDonald, S. M., Mahajan, A. S., Malpass, S., McFiggans, G., Mills, G., Misztal, P., Moller, S., Monks, P. S., Nemitz, E., Nicolas-Perea, V., Oetjen, H., Oram, D. E., Palmer, P. I., Phillips, G. J., Pike, R., Plane, J. M. C., Pugh, T., Pyle, J. A., Reeves, C. E., Robinson, N. H., Stewart, D., Stone, D., Whalley, L. K., and Yin, X.: Overview: oxidant and particle photochemical processes above a south-east Asian tropical rainforest (the OP3 project): introduction, rationale, location characteristics and tools, Atmos. Chem. Phys., 10, 169–199, doi:10.5194/acp-10-169-2010, 2010.

Hopkins, J. R., Lewis, A. C., and Read, K. A.: A two-column method for long-term monitoring of non-methane hydrocarbons (NMHCs) and oxygenated volatile organic compounds (oVOCs), J. Environ. Monit., 5, 8–13, 2003.

Hu, J. H. and Abbattt, J. P. D.: Reaction probabilities for N_2O_5 hydrolysis on sulfuric acid and ammonium sulfate aerosols at room temperature, J. Phys. Chem. A, 101, 871–878, 1997.

Jenkin, M. E., Saunders, S. M., Wagner, V., and Pilling, M. J.: Protocol for the development of the Master Chemical Mechanism, MCM v3 (Part B): tropospheric degradation of aromatic volatile organic compounds, Atmos. Chem. Phys., 3, 181–193, doi:10.5194/acp-3-181-2003, 2003.

Johnson, D. and Marston, G.: The gas-phase ozonolysis of unsaturated volatile organic compounds in the troposphere, Chem. Soc. Rev., 37, 699–716, 2008.

Kanaya, Y., Sadanaga, Y., Matsumoto, J., Sharma, U. K., Hirokawa, J., Kajii, Y., and Akimoto, H.: Nighttime observation of the HO_2 radical by an LIF instrument at Oki island, Japan, and its possible origins, Geophys. Res. Lett., 26, 2179–2182, 1999.

Kanaya, Y., Nakamura, K., Kato, S., Matsumoto, J., Tanimoto, H., and Akimoto, H.: Nighttime variations in HO_2 radical mixing ratios at Rishiri Island observed with elevated monoterpene mixing ratios, Atmos. Environ., 36, 4929–4940, 2002.

Kanaya, Y., Cao, R., Kato, S., Miyakawa, Y., Kajii, Y., Tanimoto, H., Yokouchi, Y., Mochida, M., Kawamura, K., and Akimoto, H.: Chemistry of OH and HO_2 radicals observed at Rishiri Island, Japan, in September 2003: Missing daytime sink of HO_2 and positive nighttime correlations with monoterpenes, J. Geophys. Res., 112, D11308, doi:10.1029/2006JD007987, 2007a.

Kanaya, Y., Cao, R., Akimoto, H., Fukuda, M., Komazaki, Y., Yokouchi, Y., Koike, M., Tanimoto, H., Takegawa, N., and Kondo, Y.: Urban photochemistry in central Tokyo: 1. Observed and modeled OH and HO_2 radical concentrations during the winter and summer of 2004, J. Geophys. Res., 112, D21312, doi:10.1029/2007JD008670, 2007b.

Kane, S. M., Caloz, F., and Leu, M.-T.: Heterogeneous Uptake of Gaseous N_2O_5 by $(NH_4)_2SO_4$, NH_4HSO_4 and H_2SO_4 Aerosols, J. Phys. Chem., 105, 6465–6470, 2001.

Kennedy, O. J., Ouyang, B., Langridge, J. M., Daniels, M. J. S., Bauguitte, S., Freshwater, R., McLeod, M. W., Ironmonger, C., Sendall, J., Norris, O., Nightingale, R., Ball, S. M., and Jones, R. L.: An aircraft based three channel broadband cavity enhanced absorption spectrometer for simultaneous measurements of NO_3, N_2O_5 and NO_2, Atmos. Meas. Tech., 4, 1759–1776, doi:10.5194/amt-4-1759-2011, 2011.

Lewis, A. C., Carslaw, N., Marriott, P. J., Kinghorn, R. M., Morrison, P., Lee, A. L., Bartle, K. D., and Pilling, M. J.: A larger pool of ozone-forming carbon compounds in urban atmospheres, Nature, 405, 778–781, 2000.

Lidster, R. T., Hamilton, J. F., Lee, J. D., Lewis, A. C., Hopkins, J. R., Punjabi, S., Rickard, A. R., and Young, J. C.: The impact of monoaromatic hydrocarbons on OH reactivity in the North Sea boundary layer and free troposphere, Atmos. Chem. Phys. Discuss., 13, 32423–32457, doi:10.5194/acpd-13-32423-2013, 2013.

Lunden, J., Svensson, G., Wisthaler, A., Tjernstrom, M., Hansel, A., and Leck, C.: The vertical distribution of atmospheric DMS in the high Arctic summer, Tellus, 62B, 160–171, 2010.

Macintyre, H. L. and Evans, M. J.: Sensitivity of a global model to the uptake of N_2O_5 by tropospheric aerosol, Atmos. Chem. Phys., 10, 7409–7414, doi:10.5194/acp-10-7409-2010, 2010.

Macintyre, H. L. and Evans, M. J.: Parameterisation and impact of aerosol uptake of HO_2 on a global tropospheric model, Atmos. Chem. Phys., 11, 10965–10974, doi:10.5194/acp-11-10965-2011, 2011.

Malkin, T. L., Goddard, A., Heard, D. E., and Seakins, P. W.: Measurements of OH and HO_2 yields from the gas phase ozonolysis of isoprene, Atmos. Chem. Phys., 10, 1441–1459, doi:10.5194/acp-10-1441-2010, 2010.

Martinez, M., Harder, H., Kovacs, T. A., Simpas, J. B., Bassis, J., Lesher, R., Brune, W. H., Frost, G. J., Williams, E. J., Stroud, C. A., Jobson, B. T., Roberts, J. M., Hall, S. R., Shetter, R. E., Wert, B., Fried, A., Alicke, B., Stutz, J., Young, V. L., White, A. B., and Zamora, R. J.: OH and HO_2 concentrations, sources, and loss rates during the Southern Oxidants Study in Nashville, Tennessee, summer 1999, J. Geophys. Res., 108, 4617, doi:10.1029/2003JD003551, 2003.

Mihelcic, D., Klemp, D., Musgen, P., Patz, H. W., and Volz-Thomas, A.: Simultaneous Measurements of Peroxy and Nitrate Radicals at Schauinsland, J. Atmos. Chem., 16, 313–335, 1993.

Mozurkewich, M. and Calvert, J. G.: Reaction probability of N_2O_5 on aqueous aerosols, J. Geophys. Res., 93, 15889–15896, 1988.

GLOBALVIEW-CH4, 2010–2011: Cooperative Atmospheric Data Integration Project – Methane. CD-ROM, NOAA ESRL, Boulder, Colorado, also available on Internet via anonymous FTP to ftp://ftp.cmdl.noaa.gov/ccg/ch4/, path: ccg/CH4/GLOBALVIEW, 2010–2011, last access: 24 May 2011.

Novelli, P. C., Lang, P. M., Masarie, K. A., Hurst, D. F., Myers, R., and Elkins, J. W.: Molecular hydrogen in the troposphere: Global distribution and budget, J. Geophys. Res., 104, 30427–30444, 1999.

Platt, U., Perner, D., Winer, A. M., Harris, G. W., and Pitts, J. N.: Detection of NO_3 in the polluted troposphere by differential optical absorption, Geophys. Res. Lett., 7, 89–92, 1980.

Povey, I., South, A., de Roodenbeke, A., Hill, C., Freshwater, R., and Jones, R.: A broadband lidar for the measurement of tropo-

spheric constituent profiles from the ground, J. Geophys. Res. Atmos., 103, 3369–3380, 1998.

Ravishankara, A. R.: Heterogeneous and Multiphase Chemistry in the Troposphere, Science, 276, 1058–1065, 1997.

Ren, X., Harder, H., Martinez, M., Lesher, R. L., Oliger, A., Simpas, J. B., Brune, W. H., Schwab, J. J., Demerjian, K. L., He, Y., Zhou, X., and Gao, H.: OH and HO_2 Chemistry in the urban atmosphere of New York City, Atmos. Environ., 37, 3639–3651, 2003.

Ren, X., Brune, W. H., Cantrell, C., Edwards, G. D., Shirley, T., Metcalf, A. R., and Lesher, R. L.: Hydroxyl and Peroxy Radical Chemistry in a Rural Area of Central Pennsylvania: Observations and Model Comparisons, J. Atmos. Chem., 52, 231–257, 2005.

Ren, X., Brune, W. H., Mao, J., Mitchell, M. J., Lesher, R. L., Simpas, J. B., Metcalf, A. R., Schwab, J. J., Cai, C., Li, Y., Demerjian, K. L., Felton, H. D., Boynton, G., Adams, A., Perry, J., He, Y., Zhou, X., and Hou, J.: Behavior of OH and HO_2 in the winter atmosphere in New York City, Atmos. Environ., 40, S252–S263, 2006.

Riedel, T. P., Bertram, T. H., Ryder, O. S., Liu, S., Day, D. A., Russell, L. M., Gaston, C. J., Prather, K. A., and Thornton, J. A.: Direct N_2O_5 reactivity measurements at a polluted coastal site, Atmos. Chem. Phys., 12, 2959–2968, doi:10.5194/acp-12-2959-2012, 2012.

Riedel, T. P., Wagner, N. L., Dube, W. P., Middlebrook, A. M., Young, C. J., Ozturk, F., Bahreini, R., VandenBoer, T. C., Wolfe, D. E., Williams, E. J., Roberts, J. M., Brown, S. S., and Thornton, J. A.: Chlorine activation within urban or power plant plumes: Vertically resolved $ClNO_2$ and Cl_2 measurements from a tall tower in a polluted continental setting, J. Geophys. Res. Atmos., 118, 8702–8715, doi:10.1002/jgrd.50637, 2013.

Roberts, J. M., Osthoff, H. D., Brown, S. S., Ravishankara, A. R., Coffman, D., Quinn, P., and Bates, T.: Laboratory studies of products of N_2O_5 uptake on Cl-containing substrates, Geophys. Res. Lett., 36, L20808, doi:10.1029/2009GL040448, 2009.

Salisbury, G., Rickard, A. R., Monks, P. S., Allan, B. J., Bauguitte, S., Penkett, S. A., Carslaw, N., Lewis, A. C., Creasey, D. J., Heard, D. E., Jacobs, P. J., and Lee, J. D.: Production of peroxy radicals at night via reactions of ozone and the nitrate radical in the marine boundary layer, J. Geophys. Res., 106, 12669–12687, 2001.

Sandu, A. and Sander, R.: Technical note: Simulating chemical systems in Fortran90 and Matlab with the Kinetic PreProcessor KPP-2.1, Atmos. Chem. Phys., 6, 187–195, doi:10.5194/acp-6-187-2006, 2006.

Saunders, S. M., Jenkin, M. E., Derwent, R. G., and Pilling, M. J.: Protocol for the development of the Master Chemical Mechanism, MCM v3 (Part A): tropospheric degradation of non-aromatic volatile organic compounds, Atmos. Chem. Phys., 3, 161–180, doi:10.5194/acp-3-161-2003, 2003.

Schwarz, S. E.: Mass-transport considerations pertinent to aqueous phase reactions of gases in liquid-water clouds, Chemistry of Multiphase Atmospheric Systems, NATO ASI Series, G6, Jaeschke ed., Springer-Verlag, Berlin, 415–471, 1986.

Sommariva, R., Bloss, W. J., Brough, N., Carslaw, N., Flynn, M., Haggerstone, A.-L., Heard, D. E., Hopkins, J. R., Lee, J. D., Lewis, A. C., McFiggans, G., Monks, P. S., Penkett, S. A., Pilling, M. J., Plane, J. M. C., Read, K. A., Saiz-Lopez, A., Rickard, A. R., and Williams, P. I.: OH and HO_2 chemistry during NAMBLEX: roles of oxygenates, halogen oxides and heterogeneous uptake, Atmos. Chem. Phys., 6, 1135–1153, doi:10.5194/acp-6-1135-2006, 2006.

Sommariva, R., Pilling, M. J., Bloss, W. J., Heard, D. E., Lee, J. D., Fleming, Z. L., Monks, P. S., Plane, J. M. C., Saiz-Lopez, A., Ball, S. M., Bitter, M., Jones, R. L., Brough, N., Penkett, S. A., Hopkins, J. R., Lewis, A. C., and Read, K. A.: Night-time radical chemistry during the NAMBLEX campaign, Atmos. Chem. Phys., 7, 587–598, doi:10.5194/acp-7-587-2007, 2007.

Sommariva, R., Osthoff, H. D., Brown, S. S., Bates, T. S., Baynard, T., Coffman, D., de Gouw, J. A., Goldan, P. D., Kuster, W. C., Lerner, B. M., Stark, H., Warneke, C., Williams, E. J., Fehsenfeld, F. C., Ravishankara, A. R., and Trainer, M.: Radicals in the marine boundary layer during NEAQS 2004: a model study of day-time and night-time sources and sinks, Atmos. Chem. Phys., 9, 3075–3093, doi:10.5194/acp-9-3075-2009, 2009.

Sommariva, R., Bates, T. S., Bon, D., Brookes, D. M., de Gouw, J., Gilman, J. B., Herndon, S. C., Kuster, W. C., Lerner, B. M., Monks, P. S., Osthoff, H. D., Parker, A. E., Roberts, J. M., Tucker, S. C., Warneke, C., Williams, E. J., Zahniser, M. S., and Brown, S. S.: Modelled and measured concentrations of peroxy radicals and nitrate radical in the U.S. Gulf coast region during TexAQS 2006, J. Atmos. Chem., 68, 331–362, 2011.

South, A. M., Povey, I. M., and Jones, R. L.: Broadband lidar measurements of tropospheric water vapor profiles, J. Geophys. Res. Atmos., 103, 31191–31202, 1998.

Spicer, C. W., Kenny, D. V., Chapman, E., Busness, K. M., and Berkowitz, C. M.: Observations of dimethyl sulfide over the western North Atlantic Ocean using an airborne tandem mass spectrometer, J. Geophys. Res., 101, 29137–29147, 1996.

Stone, D., Evans, M. J., Commane, R., Ingham, T., Floquet, C. F. A., McQuaid, J. B., Brookes, D. M., Monks, P. S., Purvis, R., Hamilton, J. F., Hopkins, J., Lee, J., Lewis, A. C., Stewart, D., Murphy, J. G., Mills, G., Oram, D., Reeves, C. E., and Heard, D. E.: HO_x observations over West Africa during AMMA: impact of isoprene and NO_x, Atmos. Chem. Phys., 10, 9415–9429, doi:10.5194/acp-10-9415-2010, 2010.

Stone, D., Evans, M. J., Edwards, P. M., Commane, R., Ingham, T., Rickard, A. R., Brookes, D. M., Hopkins, J., Leigh, R. J., Lewis, A. C., Monks, P. S., Oram, D., Reeves, C. E., Stewart, D., and Heard, D. E.: Isoprene oxidation mechanisms: measurements and modelling of OH and HO_2 over a South-East Asian tropical rainforest during the OP3 field campaign, Atmos. Chem. Phys., 11, 6749–6771, doi:10.5194/acp-11-6749-2011, 2011.

Stone, D., Whalley, L. K., and Heard, D. E.: Tropospheric OH and HO_2 radicals: Field measurements and model comparisons, Chem. Soc. Rev., 41, 6348–6404, 2012.

Stutz, J., Alicke, B., Ackermann, R., Geyer, A., White, A., and Williams, E.: Vertical profiles of NO_3, N_2O_5, O_3, and NO_x in the nocturnal boundary layer: 1. Observations during the Texas Air Quality Study 2000, J. Geophys. Res. Atmos., 109, D12306, doi:10.1029/2003JD004209, 2004.

Stutz, J., Wong, K. W., Lawrence, L., Ziemba, L., Flynn, J. H., Rappengluick, B., and Lefer, B.: Nocturnal NO_3 radical chemistry in Houston, TX, Atmos. Environ., 44, 4099–4106, 2010.

Tang, M. J., Thieser, J., Schuster, G., and Crowley, J. N.: Uptake of NO_3 and N_2O_5 to Saharan dust, ambient urban aerosol and soot: a relative rate study, Atmos. Chem. Phys., 10, 2965–2974, doi:10.5194/acp-10-2965-2010, 2010.

Thornton, J. and Abbatt, J. P. D.: Measurements of HO_2 uptake to aqueous aerosol: Mass accommodation coefficients and net reactive loss, J. Geophys. Res., 110, D08309, doi:10.1029/2004JD005402, 2005.

Thornton, J. A., Braban, C. F., and Abbattt, J. P. D.: N_2O_5 hydrolysis on sub-micron organic aerosols: the effect of relative humidity, particle phase, and particle size, Phys. Chem. Chem. Phys., 5, 4593–4603, 2003.

Van Doren, J. M., Watson, L. R., Davidovits, P., Worsnop, D. R., Zahniser, M. S., and Kolb, C. E.: Uptake of N_2O_5 and HNO_3 by Aqueous Sulfuric Acid Droplets, J. Phys. Chem., 95, 1684–1689, 1991.

Vaughan, S., Canosa-Mas, C. E., Pfrang, C., Shallcross, D. E., Watson, L., and Wayne, R. P.: Kinetic studies of reactions of the nitrate radical (NO_3) with peroxy radicals (RO_2): an indirect source of OH at night?, Phys. Chem. Chem. Phys., 8, 3749–3760, 2006.

Volkamer, R., Sheehy, P., Molina, L. T., and Molina, M. J.: Oxidative capacity of the Mexico City atmosphere – Part 1: A radical source perspective, Atmos. Chem. Phys., 10, 6969–6991, doi:10.5194/acp-10-6969-2010, 2010.

Walker, H. M., Stone, D., Ingham, T., Vaughan, S., Ouyang, B., Kennedy, O., McCleod, M., Jones, R. L., Hopkins, J., Punjabi, S., Lewis, A. C., and Heard, D. E.: Nighttime measurements of HO_x during the RONOCO project, in preparation, 2014.

Wagner, N. L., Riedel, T. P., Young, C. J., Bahreini, R., Brock, C. A., Dube, W. P., Kim, S., Middlebrook, A. M., Ozturk, F., Roberts, J. M., Russo, R., Sive, B., Swarthout, R., Thornton, J. A., VandenBoer, T. C., Zhou, Y., and Brown, S. S.: N_2O_5 uptake coefficients and nocturnal NO_2 removal rates determined from ambient wintertime measurements, J. Geophys. Res. Atmos., 118, 9331–9350, 2013.

Warneke, C., de Gouw, J. A., Goldan, P. D., Kuster, W. C., Williams, E. J., Lerner, B. M., Jakoubek, R., Brown, S. S., Stark, H., Aldener, M., Ravishankara, A. R., Roberts, J. M., Marchewka, M., Bertman, S., Sueper, D. T., McKeen, S. A., Meagher, J. F., and Fehsenfeld, F. C.: Comparison of daytime and nighttime oxidation of biogenic and anthropogenic VOCs along the New England coast in summer during New England Air Quality Study 2002, J. Geophys. Res., 109, D10309, doi:10.1029/2003JD004424, 2004.

Wayne, R. P., Barnes, I., Biggs, P., Burrows, J. P., Canosa-Mas, C. E., Hjorth, J., Le Bras, G., Moortgat, G. K., Perner, D., Poulet, G., Restelli, G., and Sidebottom, H.: The nitrate radical – Physics, chemistry and the atmosphere, Atmos. Environ., 25, 1–203, 1991.

Whalley, L. K., Lewis, A. C., McQuaid, J. B., Purvis, R. M., Lee, J. D., Stemmler, K., Zellweger, C., and Ridgeon, P.: Two high-speed, portable GC systems designed for the measurement of non-methane hydrocarbons and PAN: Results from the Jungfraujoch High Altitude Observatory, J. Environ. Monit., 6, 234–241, 2004.

Whalley, L. K., Blitz, M. A., Desservettaz, M., Seakins, P. W., and Heard, D. E.: Reporting the sensitivity of laser-induced fluorescence instruments used for HO_2 detection to an interference from RO_2 radicals and introducing a novel approach that enables HO_2 and certain RO_2 types to be selectively measured, Atmos. Meas. Tech., 6, 3425–3440, doi:10.5194/amt-6-3425-2013, 2013.

Wiedensohler, A., Birmili, W., Nowak, A., Sonntag, A., Weinhold, K., Merkel, M., Wehner, B., Tuch, T., Pfeifer, S., Fiebig, M., Fjäraa, A. M., Asmi, E., Sellegri, K., Depuy, R., Venzac, H., Villani, P., Laj, P., Aalto, P., Ogren, J. A., Swietlicki, E., Williams, P., Roldin, P., Quincey, P., Hüglin, C., Fierz-Schmidhauser, R., Gysel, M., Weingartner, E., Riccobono, F., Santos, S., Grüning, C., Faloon, K., Beddows, D., Harrison, R., Monahan, C., Jennings, S. G., O'Dowd, C. D., Marinoni, A., Horn, H.-G., Keck, L., Jiang, J., Scheckman, J., McMurry, P. H., Deng, Z., Zhao, C. S., Moerman, M., Henzing, B., de Leeuw, G., Löschau, G., and Bastian, S.: Mobility particle size spectrometers: harmonization of technical standards and data structure to facilitate high quality long-term observations of atmospheric particle number size distributions, Atmos. Meas. Tech., 5, 657–685, doi:10.5194/amt-5-657-2012, 2012.